MASARYKOVA UNIVERZITA
PŘÍRODOVĚDECKÁ FAKULTA
ÚSTAV TEORETICKÉ FYZIKY A ASTROFYZIKY

Diplomová práce

BRNO 2024 MATĚJ BÁRTA

MASARYKOVA
UNIVERZITA
PŘÍRODOVĚDECKÁ FAKULTA
ÚSTAV TEORETICKÉ FYZIKY A ASTROFYZIKY

Studium výtrysků molekulárního plynu v blízkých galaxiích

Diplomová práce

Matěj Bárta

Vedoucí práce: Mgr. Pavel Jáchym Ph.D. **Brno 2024**

Bibliografický záznam

Autor:	Bc. Matěj Bárta Přírodovědecká fakulta, Masarykova univerzita Ústav teoretické fyziky a astrofyziky
Název práce:	Studium výtrysků molekulárního plynu v blízkých galaxiích
Studijní program:	B-FYZ Fyzika
Studijní obor:	ASTRO Astrofyzika
Vedoucí práce:	Mgr. Pavel Jáchym Ph.D.
Akademický rok:	2023/2024
Počet stran:	xvi + 67
Klíčová slova:	Evoluce galaxií; Galaktické výtrysky; Molekulární fáze; Kosmologie; Lokální vesmír; KinMS; Spektrální datové-kostky; Rádiová spektroskopie

Bibliographic Entry

Author:	Bc. Matěj Bárta Faculty of Science, Masaryk University Department of theoretical physics and astrophysics
Title of Thesis:	Molecular gas outflows n local galaxies
Degree Programme:	B-FYZ Physics
Field of Study:	ASTRO Astrophysics
Supervisor:	Mgr. Pavel Jáchym Ph.D.
Academic Year:	2023/2024
Number of Pages:	xvi + 67
Keywords:	Galaxy evolution; Galaxy outflows; Molecular phase; Gas Dynamics; Cosmology; Local universe; KinMS; Spectral datacubes; Radio spectroscopy

Abstrakt

Galaktické výtrysky hnané aktivními galaktickými jádry a/nebo tvorbou hvězd jsou základní složkou nejmodernějších modelů vývoje galaxií založených na kosmologii Lambda CDM. Předpokládá se, že hrají klíčovou roli v regulaci efektivity tvorby hvězd v galaxiích, tvarují funkci hvězdné hmotnosti galaxie, chemické obohacování jejího prostředí a distribuci temné hmoty v galaxiích. Navzdory jejich klíčovému významu v evoluci galaxií stále chybí kompletní observační pohled. Není například jasné, která plynná fáze (ionizovaná, molekulární nebo atomová) dominuje v odtékajícím hmotnostním rozpočtu.

Hlavním cílem této práce je statisticky prozkoumat přítomnost a vlastnosti výtoků molekulárního plynu v galaktickém měřítku v lokálních galaxiích ($z \sim 0$), s cílem doplnit současný observační pohled. K dosažení tohoto cíle budou studována submilimetrová spektroskopická pozorování místních galaxií z přehlídky xCOLD GASS, s čarou CO(1-0) jako běžným indikátorem molekulární fáze. Tato pozorování budou analyzována začleněním kombinované techniky kombinování spekter a modelování čar emitovaných rotujícím diskem za účelem hledání důkazů nekruhových pohybů v galaxiích, jak je navrženo v Concas et al. 2022.

Pochopení přítomnosti a množství molekulárního plynu ve výtryskách napříč různými hvězdnými hmotnostmi jejich hostitelů je klíčovou informací pro naladění modelů vývoje galaxií a kosmologických modelů, aby lépe reprezentovaly náš vesmír.

Abstract

Galactic outflows driven by active galactic nuclei and/or star formation are a fundamental ingredient of the state-of-the-art galaxy evolution models based on the Lambda CDM cosmology. They are thought to play a key role in regulating galaxy star formation efficiency, shaping the galaxy's stellar mass function, the chemical enrichment of its environment and the dark matter distribution in galaxies. Despite their pivotal importance in galaxy evolution, a complete observational picture is still missing. For example, it is not clear which gas phase (ionized, molecular or atomic) dominates the outflow mass budget.

The main goal of this thesis is to statistically investigate the presence and properties of galactic-scale molecular gas outflows in local galaxies ($z \sim 0$), filling in the current observational picture. To achieve this goal, sub-millimeter spectroscopic observations of the xCOLD GASS sample of local galaxies will be studied, CO (1-0) line being a common tracer of the molecular phase. These observations will be analyzed by incorporating a combined stacking technique and disc-decomposition line modeling to search for evidence of non-circular motions in galaxies, as proposed in Concas et al. 2022.

Understanding the presence and amount of molecular gas in outflows across different stellar masses of their hosts is key information for constraining galaxy evolution and cosmological models to better represent our universe.

MUNI
SCI

MASARYKOVA UNIVERZITA
PŘÍRODOVĚDECKÁ FAKULTA
KOTLÁŘSKÁ 2, 611 37 BRNO
IČ: 00216224
DIČ: CZ00216224

ZADÁNÍ
DIPLOMOVÉ PRÁCE

Akademický rok: 2023/2024

Ústav:	Ústav teoretické fyziky a astrofyziky
Student:	Bc. Matěj Bárta
Program:	Fyzika
Specializace:	Astrofyzika

Ředitel *ústavu* PřF MU Vám ve smyslu Studijního a zkušebního řádu MU určuje diplomovou práci s názvem:

Název práce:	Studium výtrysků molekulárního plynu v blízkých galaxiích
Název práce anglicky:	Molecular gas outflows in local galaxies
Jazyk závěrečné práce:	angličtina

Oficiální zadání:
Galactic outflows driven by active galactic nuclei and/or star formation are a fundamental ingredient of the state-of-the-art galaxy evolution models based on the Lambda CDM cosmology. They are thought to play a key role in regulating galaxy star formation efficiency, shaping the galaxy stellar mass function, chemical enrichment of environment and dark matter distribution in galaxies. Despite their pivotal importance in galaxy evolution, a complete observational picture is still missing. For example, it is not clear which gas phase (ionized, molecular or atomic) dominates the outflows mass budget. The main goal of this project is to statistically investigate the presence and properties of galactic-scale molecular gas outflows in local galaxies (z~0), filling in the current observational picture. To achieve this goal, sub-millimeter spectroscopic observations of the xCOLD GASS sample of local galaxies will be studied, CO (1-0) line being a common tracer of molecular phase. These observations will be analyzed by incorporating stacking technique and disc-decomposition line modelling to search for evidence of non-circular motions in galaxies, as proposed in Concas et al. 2022. Understanding of the presence and amount of molecular gas in outflows across different stellar masses of their hosts is a key information for constraining galaxy evolution and cosmological models to better represent our universe.

Vedoucí práce:	Mgr. Pavel Jáchym, Ph.D.
Konzultant:	Dr. Alice Concas, Dr. Eric Emsellem
Datum zadání práce:	22. 11. 2022
V Brně dne:	6. 5. 2024

Zadání bylo schváleno prostřednictvím IS MU.

Bc. Matěj Bárta, 3. 5. 2024
Mgr. Pavel Jáchym, Ph.D., 3. 5. 2024
Mgr. Dušan Hemzal, Ph.D., 3. 5. 2024

Acknowledgements

I would like to thank my supervisor, Mgr. Pavel Jáchym Ph.D, together with my co-supervisors, Dr. Alice Concas and Dr. Eric Emsellem from European Southern Observatory, for allowing me to work on this project with their full support, guidance and neverending discussions about the topic.

I would also like to express my gratitude to the MEYS CR and the European Southern Observatory (ESO) for allowing me to spend 6 months at ESO headquarters under the joined internship program, which produced the project described in this Thesis and many potential collaborations.

Last but not least, finishing this thesis would not have been possible without support from my family, girlfriend and friends, being there for me on my way up to this point.

Declaration

Hereby I declare that I have prepared my Master's thesis independently under the guidance of the supervisor with the use of cited works.

Brno 6. května 2024 .....

Matěj Bárta

Contents

Introduction

Galaxies can have galaxy-scale winds, driving inter-stellar medium out of the galaxy, enriching the circum-galactic medium with heavy elements (e.g. Heckman et al. 2017). They are thought to be driven by stellar winds and supernovae explosions together with active galactic nuclei. The outflow of material also serves as a feedback mechanism, thought to regulate the formation of stars in galaxies by removing or preventing the collapse of dense clouds.

Feedback recipes are pivotal components of current state-of-the-art galaxy evolution models and cosmological simulations (e.g. Nelson et al. 2019). Their presence helps the results of such simulations to match the observed structures of the universe and observational parameters of galaxies, e.g. the stellar mass function, together with predicting the ubiquitous presence of outflows in local galaxies. This poses a tension between simulations and observations since such outflows are observed only in special types of galaxies, exhibiting above-average activity of star formation (e.g. McQuinn et al. 2019) and/or activity of the central black holes (e.g. King et al. 2015), while for most of the population they remain without direct proof of existence. The main reason for this may connect with the fact, that due to the small scales at which the driving mechanisms operate, they cannot be easily implemented in the simulations without significant shortcuts and simplifications.

Many studies focused on tracing the warm ionized gas in the outflows (e.g. Concas et al. 2017). Due to the multi-phase nature of the gas in the outflows, these results do not represent a complete picture of the process. In this thesis, we study the statistical characteristics of the molecular gas phase of outflows in a sample of local galaxies. The main goals are to investigate if the outflows are ubiquitous as simulations predict, and their properties.

To achieve this, we have combined stacking and disc decomposition techniques, as proposed in Concas et al. 2022, and applied them to a sample of nearby galaxies. This allows us to more reliably distinguish between the emission originating from the gaseous disc of the galaxy and that of the outflow, in contrast with other widely used techniques. Individual galaxies are modeled using physically derived models and their spectra are then extracted, mocking observation. Observations and models are compared and the mock best representing the observation is used for stacking of the spectra. The stacking step is applied to create a spectrum representing a given group of galaxies. Finally, fitting that spectrum using disc-only and disc+Gaussian models helps us assess the potential presence of perturbed motions (e.g. outflows).

Chapter 1

Galactic outflows

Figure 1.1: Composite image of galaxy M82, presenting multi-wavelength view using data from three of NASA's Great Observatories: Hubble Space Telescope (optical represented by yellow-green color and hydrogen in orange), Spitzer Space Telescope (cool gas and dust in red) and Chandra (X-rax in blue). What in optical looks like a normal galaxy is, in reality, a star-burst galaxy, creating stars around 10 times faster than our Galaxy. The rapid star formation drives massive outflows, driving gas and dust out of the galaxy. Due to its proximity, it is the best-studied example of such phenomena, serving us as a lab for testing our theories.
Credit: X-ray: NASA/CXC/JHU/D.Strickland; Optical: NASA/ESA/STScI/AURA/The Hubble Heritage Team; IR: NASA/JPL-Caltech/Univ. of AZ/C. Engelbracht

Current state-of-the-art galaxy evolution models and cosmological simulations based on ΛCDM cosmology can very closely reproduce observed large-scale structures in the universe (e.g. Springel et al. 2006). To reproduce the evolution and dynamics of individual galaxies, a feedback mechanism that can regulate star formation, either by preventing the gas from forming stars or removing it from star formation regions, is needed. Galactic outflows can represent this mechanism based on both theoretical predictions (Tomisaka et al. 1988) and actual observations (Heckman et al. 1990).

1.1 Driving mechanisms of outflows

Two main mechanisms can drive galactic-scale outflows: star-formation activity (SF feedback) and active galactic nuclei (AGNs). These two processes can inject enough energy into the interstellar medium (ISM) to allow it to escape the disc of the galaxy and create outflows.

Star formation activity plays a major role in dwarf galaxies with $\log(M_*/M_\odot) \lesssim 10.5$ (e.g. Hopkins et al. 2014), where the energy injected into the interstellar medium by stellar winds and supernovae overcomes the shallow potential well of the galaxy and allows the gas to escape.

In higher mass systems, the accretion of matter in the vicinity of the central supermassive black hole (SMBH) can result in an active galactic nuclei (AGN), releasing large quantities of energy and sometimes driving jets. This powerful mechanism can drive gas out of larger and heavier systems and is usually invoked when shaping the high mass end of the galaxy mass function (King et al. 2015).

1.2 Observations: Multi-phase nature of outflows

The interstellar medium (ISM) involves different gas phases (neutral atomic, molecular and ionized) of different temperatures and densities and dust, and they all can get expelled in the form of galactic winds.

Many existing studies are carried out with optical observations, which allow one to trace primarily the ionised phase of the gas (Hα, Hβ) together with some lines probing the neutral phase (e.g. NaD). When the results of these studies were compared with cosmological observations, it was found that only a small fraction of the mass predicted by simulations is carried in the ionized phase (e.g. Concas et al. 2022). While optical observations can provide valuable information about galactic outflows, to get a comprehensive understanding of their multiphase nature, multiwavelength studies are necessary. Only a few studies were carried out probing all the possible phases.

The relative mass contributions of the different phases in the outflows are still an open question. Some studies suggest that the majority of the gas in outflows is carried in the molecular phase, e.g. Fluetsch et al. 2021. This study was conducted using local ultraluminous infrared galaxies, galaxies undergoing starburst events, limiting the possibility of generalizing the findings for the bulk of the local population.

Chapter 2

Galaxy sample

2.1 Tracing cold gas

The most abundant molecule in the universe is the H_2 molecule. It is unfortunately challenging to directly observe since it is a highly symmetric molecule that lacks a permanent electric dipole moment. This makes it a weak rotational emitter. The lowest permitted rotational transition is $\sim 510\,\mathrm{K}$ above the ground state, which is too high for the bulk of cold molecular interstellar medium, making its intensity relatively low.

The second most abundant molecule is CO. Its excitation temperature for its lowest rotational line is $\sim 5\,\mathrm{K}$, typical for molecular clouds. This results in strong millimeter rotational lines, making it an ideal tracer of the molecular gas. The most common line CO(1-0) has frequency of $f_{CO_{10}} = 115.3\,\mathrm{GHz}$ and rest wavelength of $\lambda_{CO_{10}} = 2.6\,\mathrm{mm}$.

To convert the observed flux of the CO(1-0) line to the equivalent mass of H_2, the understanding of the CO-to-H_2 conversion factor, usually denoted α_{CO}, is an important part of interpreting the results of observations. Thanks to modern instruments like e.g. ALMA, we get robust estimates of this conversion factor together with its dependence on the environment (see Chiang et al. 2024 for a comprehensive overview of the derivation of α_{CO} from a sample of local galaxies).

2.2 xCOLD GASS survey

The xCOLD GASS ("eXtended COLD GASS") survey is a combination of two large programs carried out at the IRAM 30m telescope, providing measurements of CO (1-0) line emission for 532 galaxies in the local universe (see Saintonge et al. 2017). The main goal of these surveys was to collect a statistically significant sample of local galaxies chosen homogeneously across a given mass range, making it well-suitable for characterizing different scaling relations and their scatter. It also serves as a great reference point for studies of molecular gas content of $z \approx 0$ galaxies.

The initial program is called COLD GASS (CO Legacy Database for GASS), covering galaxies with $M_* > 10^{10}\,M_\odot$ and $0.025 < z < 0.050$. 366 galaxies were chosen at random from the complete parent sample of SDSS galaxies lying in the ALFALFA survey footprint.

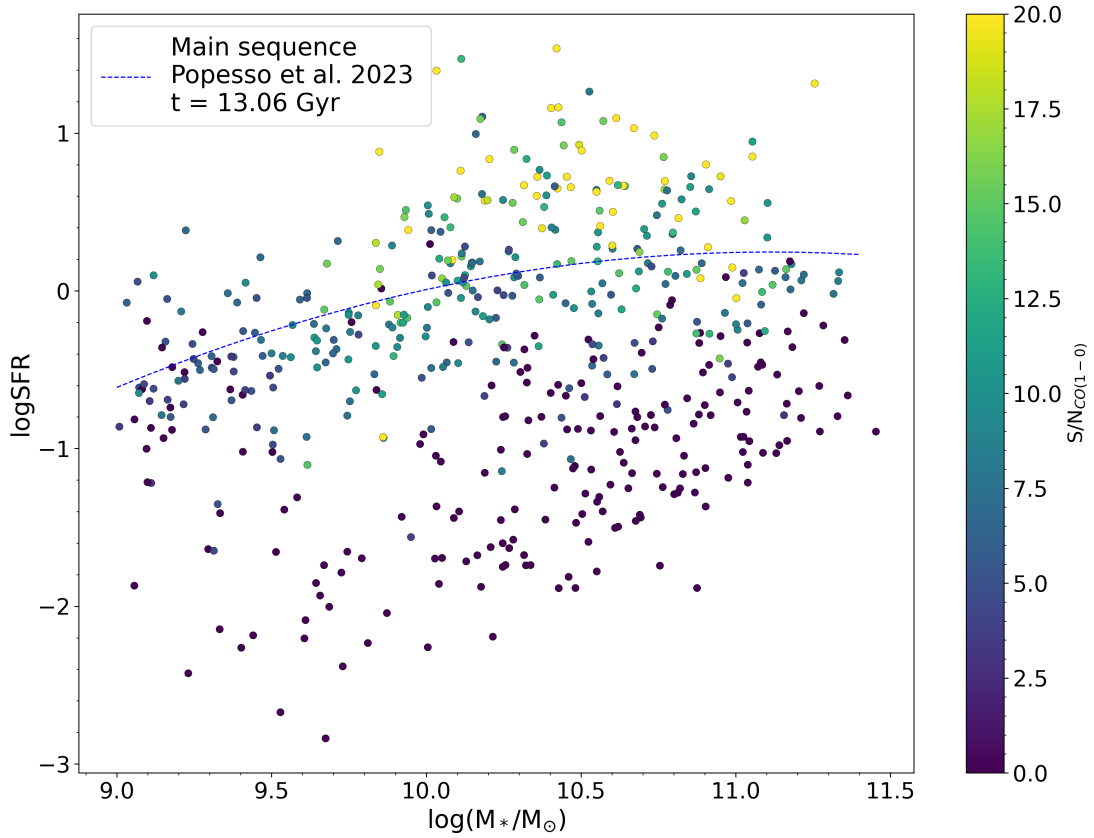

Figure 2.1: xCOLD GASS galaxies sample in M_*-SFR plot, color-coded by the signal-to-noise ratio (S/N), galaxy parameters from Saintonge et al. 2017, main sequence (MS) from Popesso et al. 2023

This makes this sample of galaxies unbiased and representative of the local population of galaxies.

The follow-up program COLD GASS-low targeted galaxies with $M_* > 10^8\,M_\odot$ and $0.01 < z < 0.02$, accounting for a lower expected CO luminosity of such galaxies. This program observed 166 galaxies randomly chosen from the SDSS parent sample containing 764 galaxies fulfilling the aforementioned criteria.

The combination of these two programs provides measurements of CO (1-0) emission for 532 local galaxies (overview of the sample is available in Figure 2.1). The CO measurements together with global galaxy properties derived from photometry were compiled in a catalog and were used in a scaling relations study by Saintonge et al. 2017. Catalog, together with spectra for individual galaxies, is available from the surveys website http://www.star.ucl.ac.uk/xCOLDGASS/.

2.3 Our sample

We base our study on a set of local galaxies observed by the xCOLD GASS survey. The study by Saintonge et al. 2017 provides observed sub-mm spectra of CO(1-0) line for 532

galaxies with 333 detections, serving as a great sample of local galaxies for statistical studies.

Because our method is based on the assumption of non-interacting galaxies, we flagged (based on visual inspection) all galaxies with deformed morphology and with close companions (e.g. Figure 2.2), to avoid observed spectra that are a combination of emission from two galaxies. After we removed these galaxies, we identified spectra with a signal that was strong enough for our study: more specifically, we required the spectra to have the mean flux within the W50 range (specified in the Saintonge et al. 2017 catalog) above a certain value, specifically with:

$$\text{mean}(f_{\text{W50}}) \geq 1.5$$

This value ensures that the mean flux of the line lies above most of the surrounding noise, increasing confidence in model fitting.

Our final sample contains 226 galaxies, with $9.0 \leq \text{M}_* \leq 11.5$. The sample is visualized in Figure 2.4, while an example of the included galaxies is in Figure 2.3, containing the SDSS image and spectrum from xCOLD GASS survey, all taken from Saintonge et al. 2017. A list of all included galaxies together with model parameters are in Appendix section A.

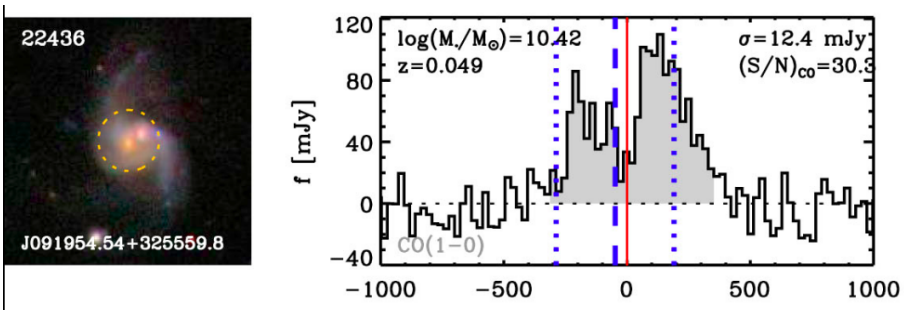

(a) Example of interacting galaxy in the xCOLD GASS sample

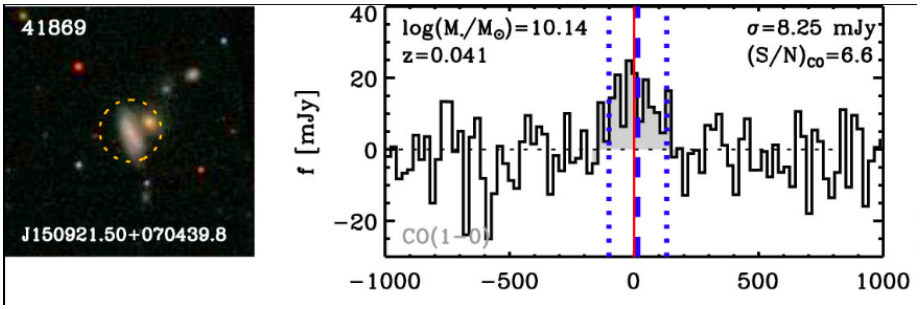

(b) Example of the galaxy with a close companion in the xCOLD GASS sample

Figure 2.2: Example of galaxies flagged due to the merger/companion criterium. Each figure shows SDSS image and CO(1-0) spectrum from xCOLD GASS survey corrected for SDSS redshift. The blue dashed line corresponds to the redshift of CO(1-0) line, the blue dotted line shows the W_{50} range. Similar figures for all the galaxies in xCOLD GASS sample are available from Saintonge et al. 2017

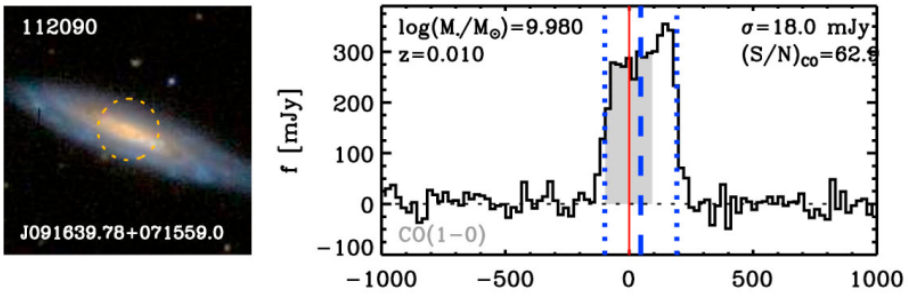

(a) Example of galaxy with high signal-to-noise factor, $S/N = 13.4$

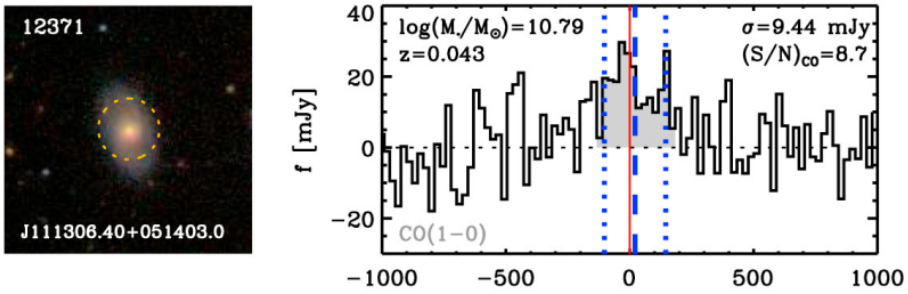

(b) Example of galaxy with low signal-to-noise factor, $S/N = 1.6$

Figure 2.3: Example of galaxies included in our study. Each figure shows SDSS image and CO(1-0) spectrum from xCOLD GASS survey corrected for SDSS redshift. The blue dashed line corresponds to the redshift of CO(1-0) line, the blue dotted line shows the W_{50} range. Similar figures for all the galaxies in our sample are available from Saintonge et al. 2017

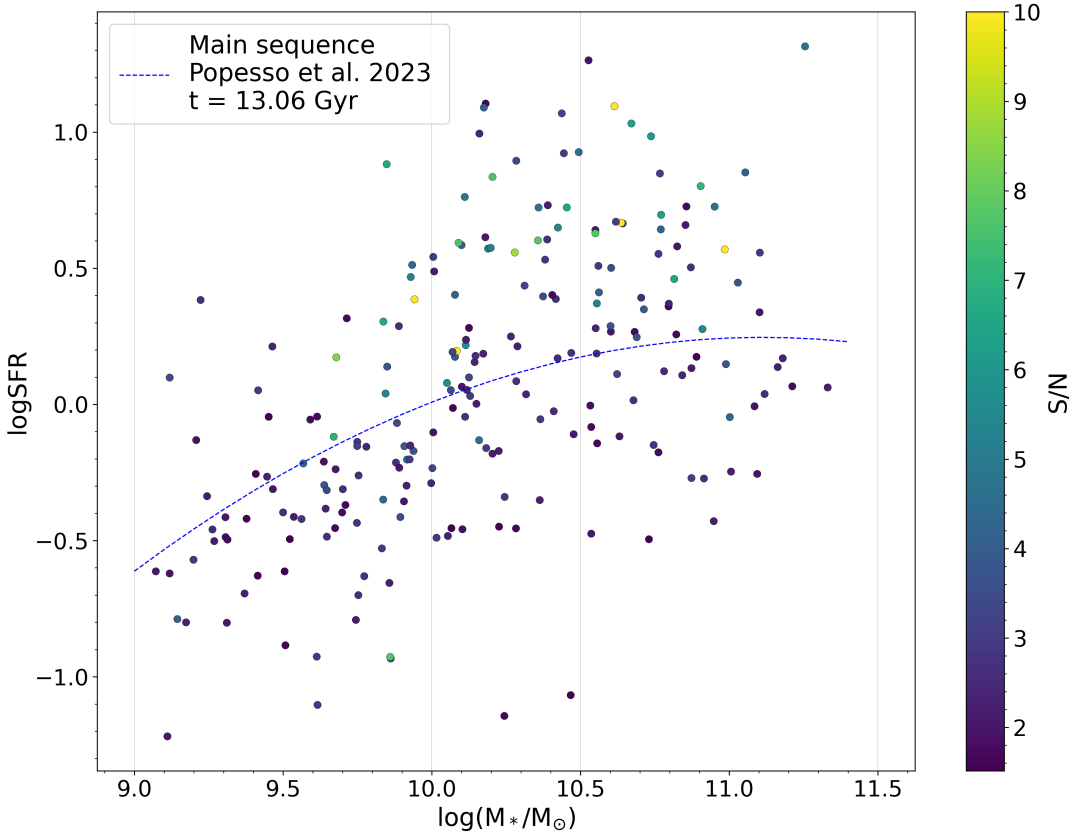

Figure 2.4: SFR-M_* diagram of our final sample, color-coded by the S/N as described in section 2.3, limited to the maximum of 10 (only a few galaxies lie above this threshold). Vertical grey lines are dividing the mass range into 3 bins, later used for the stacking of spectra.

Chapter 3

Searching for outflows

Depending on the type of observed data, different methods are commonly used to search for galactic outflows. With spatially resolved observations, individual deviating flux sources can be identified, while in the case of integrated (e.g., aperture) spectroscopy, we only have the integrated kinematic properties of the galactic target. In the latter case, which is used in our study, we have to define a way how to separate the emission of the ISM that is bound to the galaxy from the potential outflow.

A widely used method (as found in e.g. Genzel et al. 2014) is based on the assumption that the spectral line of the galaxy can be divided into two distinguishable components - a narrow Gaussian component, tracing the rotation and turbulent motion inside the galaxy, and a broad Gaussian component, representing the non-circular motion. The main advantage of this method is its simplicity and quick applicability, the fitting is not constrained by any physical parameters of the observed galaxy but depends only on the assumption made for the limits of FWHM of the individual components. This also presents one of the main disadvantages of the method: since there is no straightforward way how to select the width criteria, it varies in different studies, which brings inconsistency in the process and leads to possible misinterpretation of the results.

A closer look at the spectra of individual galaxies reveals that the assumption of a strictly Gaussian-like shape of the line is not applicable in general. In Figure 3.1, it can be seen that the shape of the line is dependent on the inclination and stellar mass of the galaxy. In case of a high inclination and high stellar mass, the single Gaussian-like shape splits into two distinct peaks connected by a 'valley', creating the so-called double horn profile, unobtainable by the simple Gaussian model. Moreover, when spectral lines with different widths and shapes are stacked, the resulting shapes may look like being composed of two Gaussian-like profiles, suggesting falsely the presence of an outflow.

3.1 Disc decomposition method

To overcome the difficulties connected to the use of double Gaussian decomposition when searching for outflows in galaxy-integrated spectra, we use the physically motivated disc decomposition technique combined with spectral stacking recently proposed by Concas et al. 2022. The basis of the method is to create a model of the emission of a rotating disc component, make mock observations of the simulated emission line, and compare

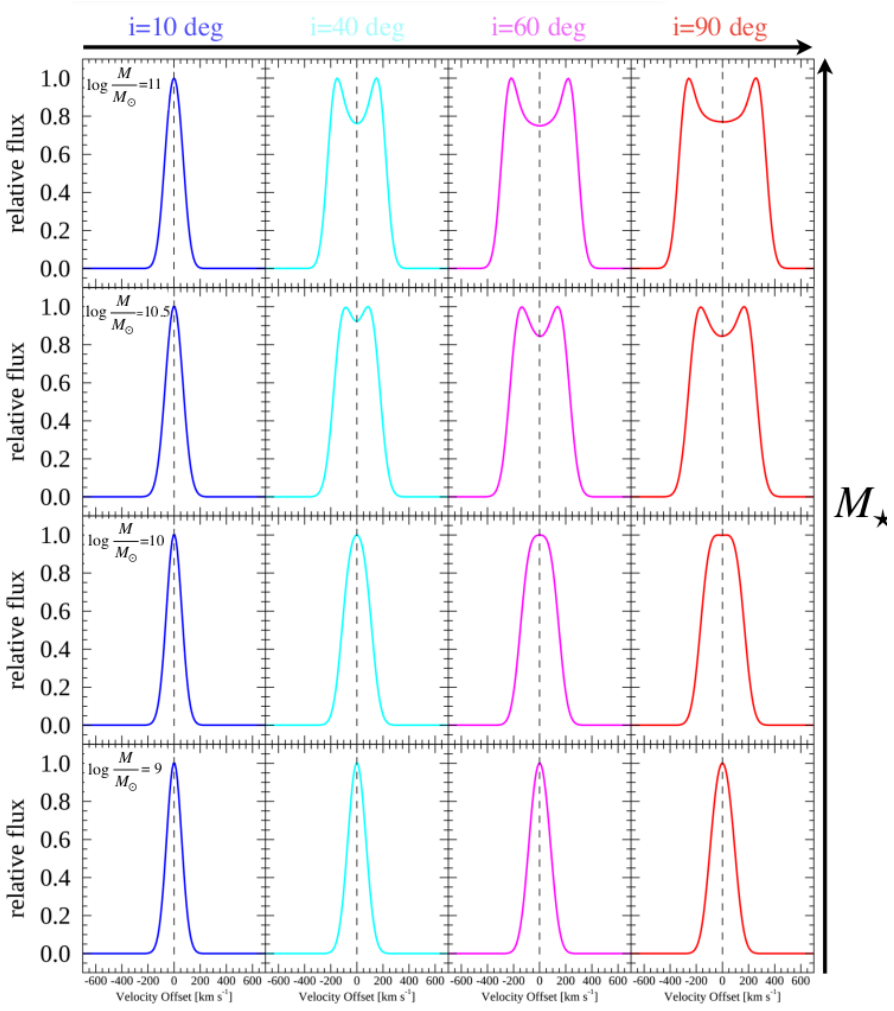

Figure 3.1: Examples of spectral profile shapes corresponding to different inclinations and masses of the galaxy. Going to higher inclination (right) and higher masses (up) reveals a double-horn profile, clearly not representable by the simple double-Gaussian method. Taken from Concas et al. 2022.

it with the observed spectrum. To produce statistical results, as well as to improve the signal-to-noise ratio (S/N) in the wings of the line, stacking multiple spectra is incorporated.

We employ this method in our study, with minor changes to the individual steps, to adapt it to our dataset. The description of the precise methodology follows in this chapter.

3.2 Spectra pre-processing

Before the spectra from the xCOLD GASS survey can be used in our method, we have to carry out two important steps.

First, we have to correct the spectra for redshift, so that we can directly stack them without introducing any systematic shifts that could be mistaken for outflows. The Saintonge et al. 2017 catalog contains redshift values from the SDSS survey (optical), as well

as the redshifts derived from fitting the observed CO lines. We used the latter for the redshift correction of the observations, as Saintonge et al. 2017 showed a minor discrepancy between the two redshifts.

The shift to the rest frame was achieved through two steps. First, we used the relation connecting the observed and rest frequency

$$f_{\mathrm{rest}} = (1+z) f_{\mathrm{obs}} \tag{3.1}$$

where z is the redshift of the CO line determined by Saintonge et al. 2017 and $c = 299\,792\,458\,\mathrm{m\,s^{-1}}$ is the speed of light. Then we calculated the corresponding velocities of observation, using the 'radio' Doppler shift convention

$$v_{\mathrm{obs}} = c \left(1 - \frac{f_{\mathrm{obs}}}{f_{\mathrm{rest}}} \right) , \tag{3.2}$$

where $f_{\mathrm{rest}} = 115.27\,\mathrm{GHz}$ is the rest frame frequency of the CO (1-0) transition.

For easier stacking of the spectra and creation of the models, we also resampled all spectra to a common velocity grid. The sampling was selected to be $\Delta v = 11\,\mathrm{km\,s^{-1}}$, which corresponds to the mean sampling found across the raw data. The resampling was done using linear interpolation, assuming a linear change of flux between the neighboring points. An example of the resampling can be seen in Figure 3.2, which shows that this resampling method may create slight systematic errors within the spectrum. These errors however lie within the noise of the original spectrum and given the statistical nature of our approach, their effect on the results is negligible.

As part of the processing of all the spectra we also quantified the RMS of the measured fluxes (=noise) in close vicinity of the line, in regions $v \in [-900, -600]\,\mathrm{km\,s^{-1}}$ and $v \in [600, 900]\,\mathrm{km\,s^{-1}}$, and the S/N of the line as the mean flux inside the W50 range from xCOLD GASS catalog divided by the RMS noise for each galaxy. These values were saved for later use alongside the values from Saintonge et al. 2017 catalog.

All pre-processed spectra were saved in a machine-readable format, containing a brief description of the data and velocity and flux values, limited to $v \in [-2200, 2200]\,\mathrm{km\,s^{-1}}$, centered on $v = 0\,\mathrm{km\,s^{-1}}$.

3.3 Mock galaxies

The principal step of our method is the creation of mock CO (1-0) galaxy-integrated spectral lines. To obtain these models, we need to first create a spectral cube representing the CO (1-0) emission of a rotating molecular disc, and then extract an integrated spectrum from the cube.

Before we can start creating the mock spectral cubes, two profiles characterizing rotating discs need to be defined – the surface-brightness profile (= radial distribution of the emitting material) and the velocity profile. The next two subsections present the specific profiles used for our modeling, while the third describes the values used in the calculations for individual galaxies.

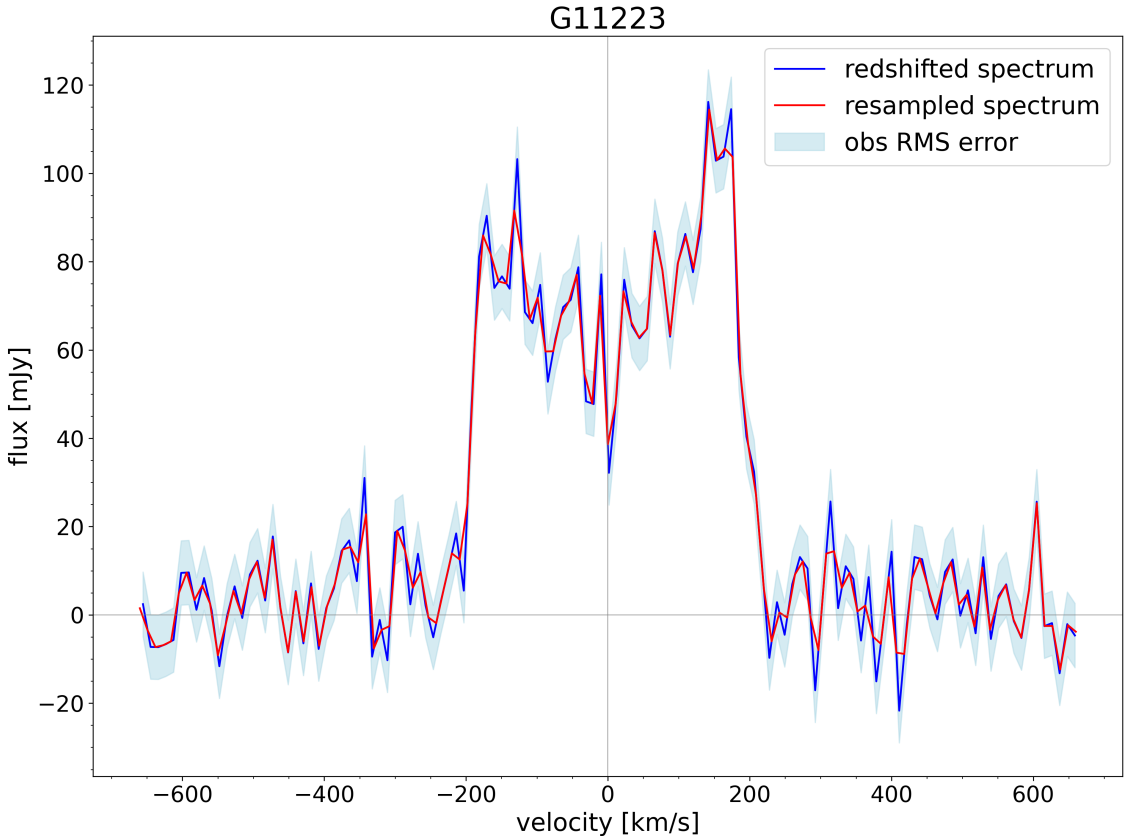

Figure 3.2: Comparison of the observed spectra before (blue line) and after (green line) resampling. It can be seen that the error induced by the used interpolation lies within the noise, creating negligible differences in the line shape.

3.3.1 Surface brightness profile

The surface brightness profile describes the distribution of intensity as a function of distance from the galaxy center. The most widely used profile is the Sérsic profile (Sérsic 1963), a result of the generalization of profiles used to approximate the surface brightness profile of galaxies. The Sérsic profile is typically used in the following form:

$$I(R) = I_e \exp\left\{-b_n\left[\left(\frac{R}{R_e}\right)^{1/n} - 1\right]\right\}, \tag{3.3}$$

where R_e is the so-called 'half-light radius', containing 50% of the total luminosity; I_e is the intensity achieved at R_e, n the Sérsic index controlling the slope of the distribution; and the coefficient b_n, normalizing the exponential, can be found as $\gamma(2n;b_n) = \frac{1}{2}\Gamma(2n)$.

The most widely used Sérsic indexes are $n = 1$, corresponding to exponential profile, used to approximate spiral galaxies, and $n = 4$, also known as de Vaucouleurs profile (de Vaucouleurs 1948), used to approximate typical elliptical galaxies. In our case, the distribution of the CO emission can be approximated by a thin exponential disc (see Bolatto et al. 2017), corresponding to $n = 1$.

3.3.2 Velocity profile

Velocity profiles were calculated by considering the gravitational potentials of individual components of the galaxy: stellar, gaseous and Dark Matter Halo (DMH). The stellar component is composed of two parts - a bulge and a disc. An example of this approach can be seen in Di Cintio et al. 2016.

For the stellar bulge, we use Hernquist potential (Hernquist 1990). The radial density distribution $\rho(r)$ is described as

$$\rho(r) = \frac{A}{4\pi a^3} \frac{1}{(r/a)(1+r/a)^3} , \tag{3.4}$$

where A is the amplitude of the potential, in our case $2M_{\text{bulge}}$ and a is the scale radius of the bulge ($r_{1/4}$). We calculated the circular velocity of the bulge by using the `galpy` package (Bovy 2015, `http://github.com/jobovy/galpy`), first initializing the potential by defining the amplitude $A = 2M_{\text{bulge}}$ and scaling radius $r_{1/4}$ and then utilizing the `calcRotcurve` method (see section B).

The stellar disc is well described by a thin exponential disc potential (Freeman 1970). The circular velocity of this potential can be calculated as

$$v^2_{\text{disc}}(r) = \frac{2GM_{\text{disc}}}{r_{\text{disc}}} y^2 (I_0(y)K_0(y) - I_1(y)K_1(y)) , \tag{3.5}$$

where M_{disc} is the total mass of the disc, $G = 4.3 \cdot 10^{-3}\,\text{pc}\,\text{M}_\odot{}^{-1}\,\text{km}^2\,\text{s}^{-2}$ is the gravitational constant, r_{disc} the scaling radius of the disc, $y = r/2 * r_{\text{disc}}$ is the normalized radius r at which the velocity is calculated, and I_n and K_n are the nth-order modified Bessel functions.

For the gaseous disc, we assume a thin exponential disc with a scaling radius $r_{\text{gas}} = 2r_{\text{disc}}$. The velocity profile of the gas disc is calculated using the same equation as for the stellar disc (3.5).

To account for the DMH, we include a Navarro-Frenk-White (NFW) potential (Navarro et al. 1996). The circular velocity profile of NFW potential can be expressed as

$$v^2_{\text{DMH}} = \left(\frac{c_{200}}{x} \left[\left(\ln(1+x) - \frac{x}{(1+x)} \cdot \frac{1}{\ln(1+c_{200}) - \frac{c_{200}}{1+c_{200}}} \right) \right] \right) v^2_{200} , \tag{3.6}$$

where $c_{200} = 200 c_{\text{crit}}$ is the mean concentration inside the virial radius r_{200}, $x = r/R_{\text{DMH}}$ is the normalized radius in units of DMH scaling radius and v_{200} is the circular velocity at r_{200}.

After the circular velocity profiles of all individual components were calculated, we combined them using the relation

$$v^2_{\text{circ}} = v^2_{\text{bulge}} + v^2_{\text{disc}} + v^2_{\text{gas}} + v^2_{\text{DMH}} . \tag{3.7}$$

This gave us the total circular velocity profile of the galaxy that takes into account all its components.

3.3.3 Parameters of individual galaxies

To create models representing the galaxies in our sample, we need to characterize each galaxy with a set of parameters given in Table 3.1.

	Parameter	Used for
r_{SB}	surface brightness scaling radius	surface brightness profile
$r_{\mathrm{disc,\ stellar}}$	scaling radius of stellar disc	velocity profile
$M_{\mathrm{disc,\ stellar}}$	mass of the stellar disc	velocity profile
$r_{\mathrm{disc,\ gas}}$	scaling radius of gas disc	velocity profile
$M_{\mathrm{disc,\ gas}}$	mass of the gas disc	velocity profile
$r_{1/4,\mathrm{bulge}}$	scaling radius of bulge	velocity profile
M_{bulge}	mass of the gas disc	velocity profile
M_{DMH}	mass of the dark matter halo	velocity profile
inc_{kin}	inclination of the galaxy	direct model input

Table 3.1: Parameters needed for reproducing galaxy during modeling

The values of these parameters can be deduced for each galaxy from quantities available from three catalogs - Saintonge et al. 2017 (xCOLD GASS), Catinella et al. 2018 (xGASS - HI survey) and Simard et al. 2011 (bulge+disc decomposition). We cross-matched these catalogs using the TOPCAT software (Taylor 2005) and exported the parameter values from the three sources into a new, concise catalog. The individual quantities used to calculate the parameters from Table 3.1, together with the used relations are summarized in Table 3.2.

However, the Catinella et al. 2018 and Simard et al. 2011 catalogs do not cover all the galaxies from our sample. Specifically, Catinella et al. 2018 provides M_{HI} for only 191 galaxies from our sample. We therefore had to quantify the gas content of the remaining 35 galaxies using scaling relations for the quantities that are available from the xCOLD GASS catalog. For all the galaxies with molecular gas content measurements in Saintonge et al. 2017 (xCOLD GASS) and atomic gas in Catinella et al. 2018 (xGASS), we used a linear fit to derive a relation for the total gas content M_{gas} as a function of the stellar mass in the form

$$\log(M_{\mathrm{gas}}/\mathrm{M}_{\odot}) = 0.45 * \log(\mathrm{M}_{*}/\mathrm{M}_{\odot}) + 5.15\ , \tag{3.8}$$

where M_{stellar} is the stellar mass available from the Saintonge et al. 2017 catalog. The relation is shown in Figure 3.3, together with the relation for $\mathrm{M_{HI}}$ and $\mathrm{M_{H2}}$ separately. We decided to use the relation for the total gas content M_{gas} instead of only quantifying the M_{HI} and adding it to the M_{CO}, as we are mainly interested in the total gas content and both methods gave consistent results.

Furthermore, the Simard et al. 2011 catalog covers only 196 galaxies, for the remaining 30 galaxies we had to quantify 4 parameters: $(B/T)_r$, R_d, R_e and $scale$. The first mentioned, $(B/T)_r$, showed a tight relation with the concentration index cindx $= R_{90,r}/R_{50,r}$ available in Saintonge et al. 2017 catalog (see Figure 3.4). We chose to do a reverse linear fitting, as the change in $cindx$ may not result from higher $(B/T)_r$. The used relation has the following form

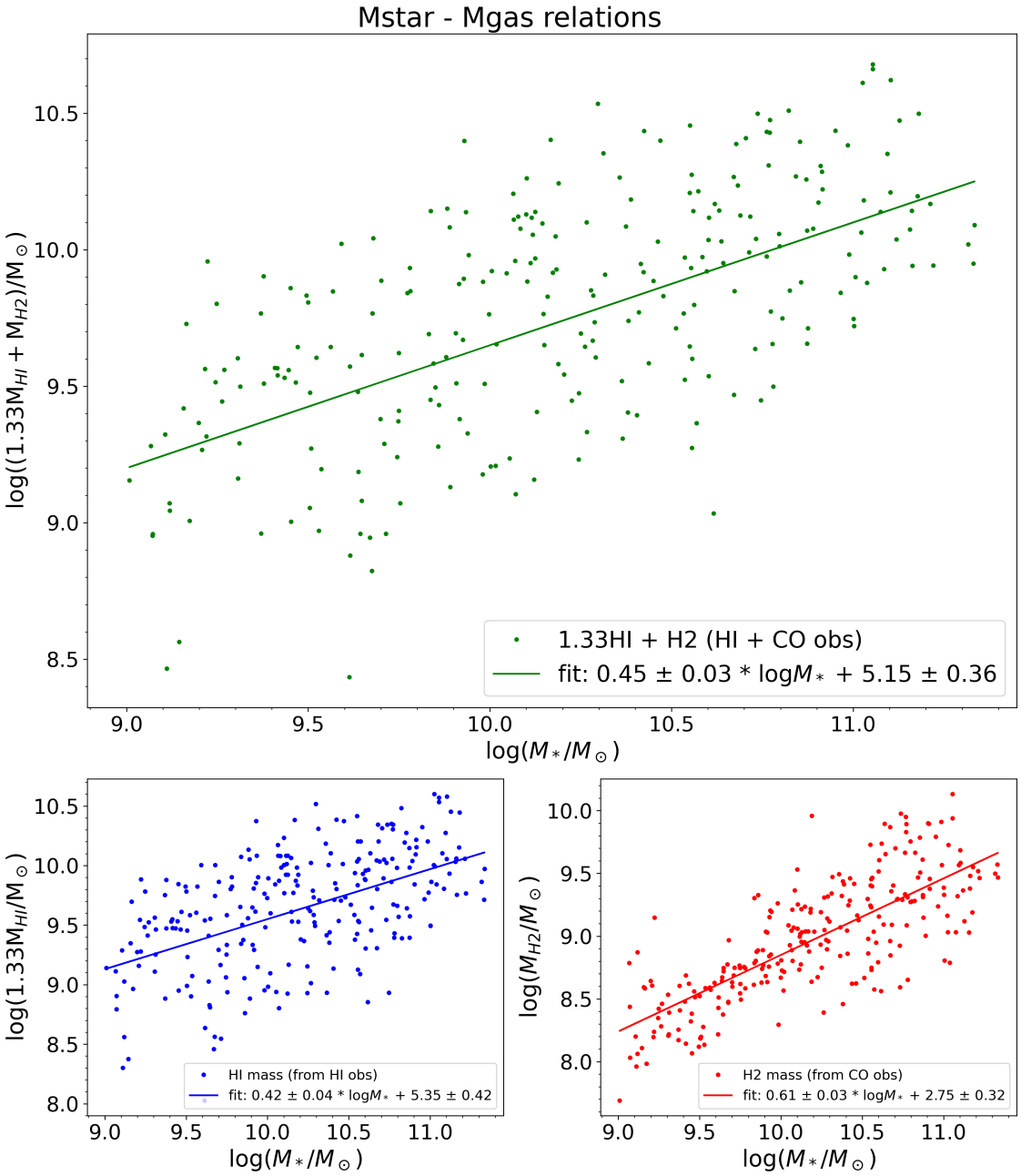

Figure 3.3: Relation between the stellar mass M$_*$ and the HI (lower left panel), H_2 (lower right panel), and M_{gas} (upper panel) for the galaxies from the xCOLD GASS survey (Saintonge et al. 2017) with HI masses available from xGASS survey (Catinella et al. 2018). The factor of 1.33 applied to the HI mass accounts for the Helium content (see Di Cintio et al. 2016).

Relation	Main source
$r_{SB} = r_{50,\mathrm{kpc}}/scale$	r_{50}: Saintonge et al. 2017, *scale*: Simard et al. 2011 relation based on results of Bolatto et al. 2017
$r_{\mathrm{disc,\ stellar}} = R_d/scale$	both Simard et al. 2011
$M_{\mathrm{disc,\ stellar}} = M_{\mathrm{stellar}} * (1-(B/T)_r)$	M_{stellar}: Saintonge et al. 2017, $(B/T)_r$: Simard et al. 2011
$r_{\mathrm{disc,\ gas}} = 2 * r_{\mathrm{disc,\ stellar}}$	
$M_{\mathrm{disc,\ gas}} = 1.33 * M_{HI} + M_{CO}$	M_{HI}: Catinella et al. 2018, M_{CO}: Saintonge et al. 2017 , factor 1.33 accounts for Helium content (see Di Cintio et al. 2016)
$r_{1/4,\mathrm{bulge}} = R_e/[(1+\sqrt{2}) * scale]$	R_e: Simard et al. 2011
$M_{\mathrm{bulge}} = M_{\mathrm{stellar}} * (B/T)_r$	$(B/T)_r$: Simard et al. 2011
$M_{\mathrm{DMH}} \propto M_{\mathrm{stellar}}$	precise relation from Moster et al. 2013
$inc_{\mathrm{kin}} = \arcsin W50_{CO}/(2 * v_{\mathrm{max}})$	$W50_{CO}$: Saintonge et al. 2017, v_{max}: maximum velocity inside $r =$ 20 arcsec in velocity profile

Table 3.2: Relations used to calculate model parameters for galaxies. $r_{50,kpc}$ is the half-light radius, $scale[\mathrm{arcsec}^{-1}]$ is the conversion factor from angular to physical units, R_d is the scale radius of the stellar disc, $(B/T)_r$ is the bulge fraction, M_{HI} is the total HI mass, M_{CO} is the total molecular mass, R_e is the scale radius of bulge, $W50_{CO}$ is the FWHM of the CO line and v_{max} corresponds to maximum velocity achieved inside $r = 20$ arcsec in velocity profile.

$$(B/T)_r = \frac{cindx - 2.17}{1.36} \ . \tag{3.9}$$

As this relation can return a negative value, in such case it is set to $(B/T)_r = 0$.

Secondly, we quantified R_d and R_e based on their relation with R_{50} (see Figure 3.5) in the form

$$R_d = 1.08 * R_{50} \tag{3.10}$$
$$R_e = 0.69 * R_{50} \tag{3.11}$$

Lastly, we calculated the last missing parameter, *scale*, from the geometric equation for cosmology. In our case, we used an approximate equation valid for $z \sim 0$

$$scale \approx \frac{1}{\deg\left(\frac{(1+z)^2}{D_{\mathrm{lum}}}\right) * 3600} \tag{3.12}$$

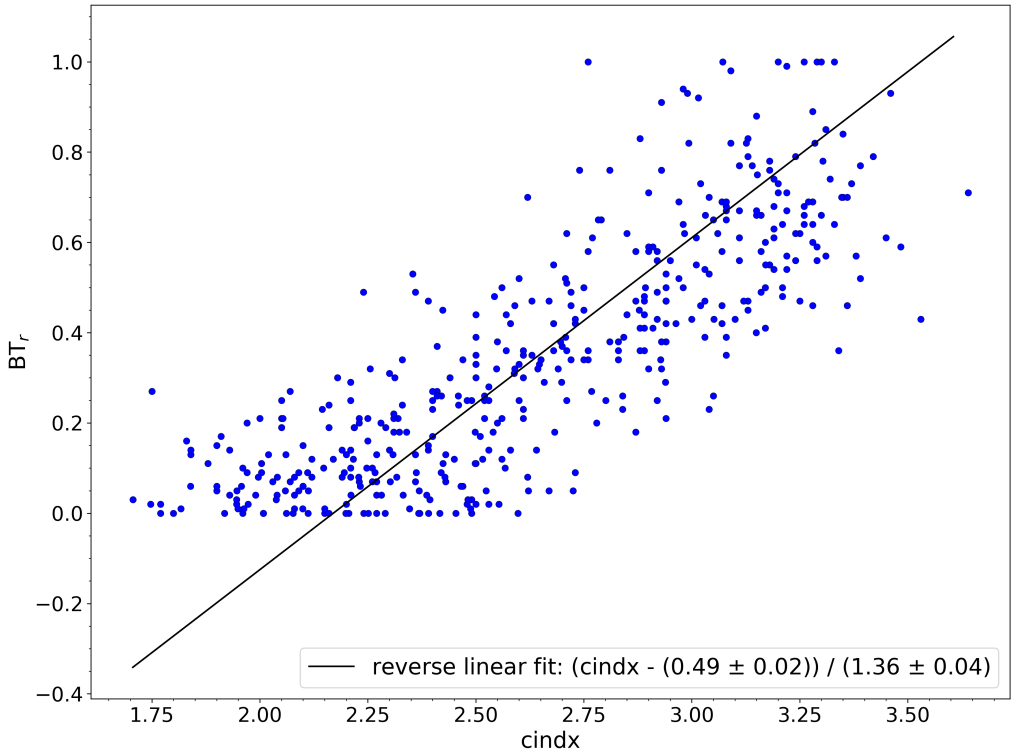

Figure 3.4: Relation between *cindx* from Saintonge et al. 2017 and B/T_r from Simard et al. 2011 for xCOLD GASS galaxies covered by both catalogs.

where z is the redshift of galaxy and $D_{\rm lum}$ luminosity distance of the galaxy from Saintonge et al. 2017 catalog. We used $D_{\rm lum}$ in units of kpc so that we got the resulting scale factor in units of [kpc arcsec^{-1}].

The values of the model parameters for individual galaxies are reported in Appendix section A.

3.3.4 Mock spectral cubes

With the galaxy parameters and profiles quantified, we were able to create model spectral cubes simulating integral field unit (IFU) observations of the galaxies. To achieve this we utilized `KinMS` python package inside a custom written Python class (which can be seen in Appendix section B).

The `KinMS` package (KINematic Molecular Simulation (KinMS) routine of Davis et al. 2013) is broadly used to model 3D datacubes with two spatial and one spectral axis, simulating interferometer or IFU observations. The cubes are created based on the surface brightness profile and velocity profile. The code also accounts for observational effects by convoluting the ”clean” datacube with the beam/point spread function (PSF) of the instrument.

The process of a datacube creation has two steps. In the first step, the parameters of the data cube that we want to return are set, specifically the physical dimensions, channel width, and beam size. In our case we used values described in Table 3.3.

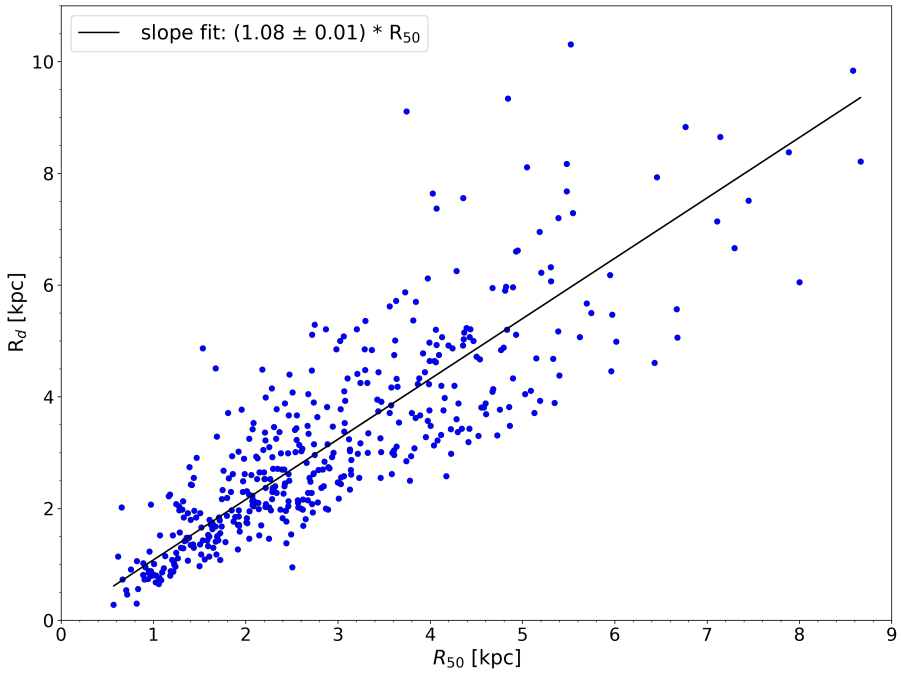

(a) Relation between R_{50} from Saintonge et al. 2017 and R_d from Simard et al. 2011 for the xCOLD GASS galaxies covered by both catalogs.

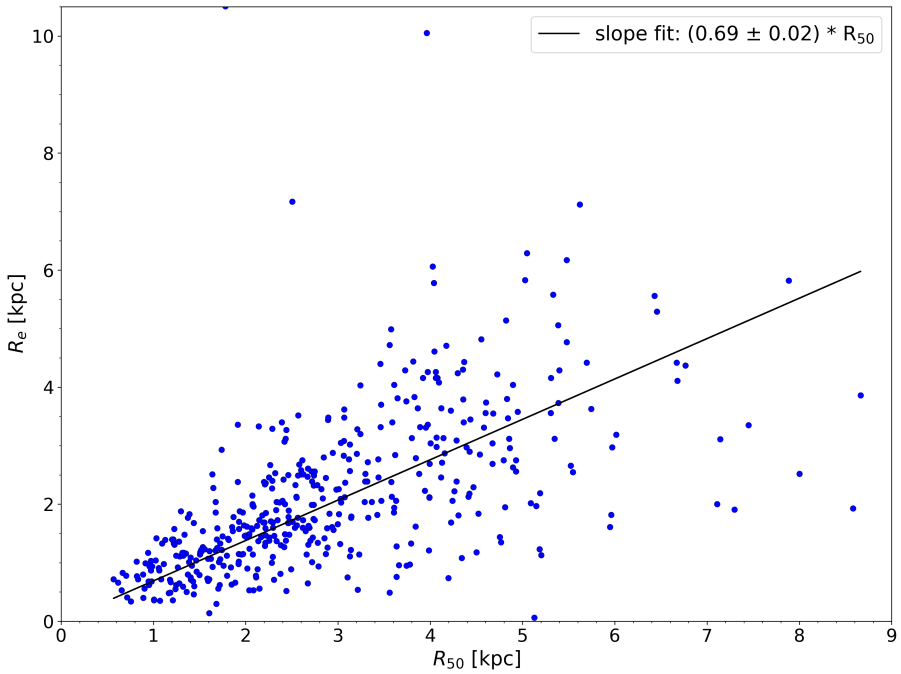

(b) Relation between R_{50} from Saintonge et al. 2017 and R_e from Simard et al. 2011 for the xCOLD GASS galaxies covered by both catalogs.

Figure 3.5: Relations used to quantify the scaling radius of stellar disc R_d and bulge $R_{\rm bulge}$ for galaxies not covered by Simard et al. 2011

Parameter	Value used
xs	105 px
ys	105 px
vs	881 $\mathrm{km\,s^{-1}}$
cellSize	1 $\mathrm{arcsec\,px^{-1}}$
dv	11 $\mathrm{km\,s^{-1}}$
beamSize	(22×22) arcsec

Table 3.3: Cube parameters used for creation of all galaxy model data cubes from KinMS, passed at initialization of the KinMS class. xs and ys are the angular sizes of datacube in x/y axis, vs is the size of the velocity axis, cellSize is the spatial resolution of the cube, dv the spectral resolution, beamSize specifies the beam to convolved the cube with.

In the second step, we initialize the modeling of the datacube by calling the `KinMS.model_cube` method. In this step, the surface brightness profile and the velocity profile, together with the other parameters of the desired model, are entered as arguments. The list of the used arguments is available in Table 3.4. We used `restFreq` = $f_{CO(1-0)}$ = 115.27 GHz and `gasSigma` = σ_{CO} = 10 $\mathrm{km\,s^{-1}}$, consistent with the results of the studies of local galaxies, e.g. Bacchini et al. 2020.

Argument	Description
`sbRad`	radial values array [in arcsec]
`sbProf`	surface brightness profile array
`velProf`	velocity profile array
`inc`	inclination of the galaxy
`posAng`	position angle of the galaxy
`restFreq`	rest frequency of the observed line
`gasSigma`	velocity dispersion of the gas

Table 3.4: Arguments passed to KinMS.model_cube method to produce datacube representing galaxy with specified parameters

3.3.5 Integrated spectra extraction

To extract an integrated spectrum from the mock datacube, we utilized the Python package `spectral_cube` (see Ginsburg et al. 2019), designed for manipulation and analysis of spectral datacubes containing two spatial and one spectral axis.

In our case, we needed to create integrated spectra to mimic single-dish observations carried out during the xCOLD GASS survey. First, we defined a circular aperture with the radius $r_{\mathrm{aperture}} = 26$ arcsec, limiting the area that we integrated the flux from. This radius was chosen based on the fact that the mock cube is already convolved with the beam of the single-dish telescope, smearing the emission from individual clouds. A single dish beam with $FWHM = 22$ arcsec reaches its first null at $r_{\mathrm{null}} \approx 13$ arcsec, the majority of the emission originating from within this circle after convolution will be spread inside an area with $r = 26$ arcsec.

After applying the circular aperture mask, the integrated spectrum was extracted as the sum of all fluxes inside the aperture for each channel. The resulting spectra are saved into text files with columns containing velocity channels and corresponding fluxes.

3.3.6 Mocks fitting

After we created each model spectrum we fitted it to the observation. To be able to fit it to the observations, we used `numpy.interp` method to create a function from the modeled vfluxes, then it was fitted to the observations by the `scipy.optimize.curve_fit`. We were fitting two parameters, A the scaling of the model spectrum, since the flux of the models was not normalized during creation, and the shift in velocity v_0 to align the observation and the mock, negating any possible systematic velocity shift due to uncertainties.

After fitting, each model is assigned a chi^2 value, based on the equation

$$chi^2 = \sum_{i=0}^{N} \frac{(f_{i,\mathrm{obs}} - f_{i,\mathrm{model}})^2}{\mathrm{RMS}_{\mathrm{obs}}^2} , \tag{3.13}$$

where $f_{i,\mathrm{obs}}$ is the observed flux at i-th channel, $f_{i,\mathrm{model}}$ is the flux of the model fit at i-th channel, and $\mathrm{RMS}_{\mathrm{obs}}$ is the quantification of the noise surrounding the line, as described in section 3.2. The value for the model was saved together with the parameters used.

3.3.7 Finding the best mocks

To find the best-fit model we created several realizations of the model, changing the inclination of the galaxy (inc) and the surface brightness scaling radius (r_{SB}) to create different versions. For the inclination, we decided to create a range of 9 values, centered on the inc_{kin} as the initial guess. We calculated the inclination range such that each step in inclination represents a change in the width of the line $dW = 11\,\mathrm{km\,s^{-1}}$. This allows us to create a wide range of inclinations. We achieved it by first calculating the range of $\sin i$ since it is linear with the change of $W50$. The formula for this is

$$\sin i_n = \frac{W50 + n\,dW}{2v_{\mathrm{max}}} , n \in \mathbb{N} , \tag{3.14}$$

where $W50$ is the initial line width, in our case it is $W50_{CO}$ from Saintonge et al. 2017 catalog, dW the desired change in the linewidth, v_{max} maximum velocity as in Table 3.1 and $n \in [-4,-3,...,0,...,3,4]$ to represent the 9 variants. After calculating the $\sin i$ range we discarded values outside of the permitted value range of $\sin i \in [0,1]$. If the border was crossed we included the border value $\sin i = 0$ or 1 instead of one of the values lying outside of it. Finally, we calculated corresponding values of inclination by applying arcsin on the generated range.

For the surface brightness scaling radius r_{SB}, we decided to create a range of 4 values by multiplying the initial value of r_{SB} (see Table 3.1) by factors of [0.5, 1, 2, 3]. The initial value is based on the empirical relation between stellar and molecular components (see Bolatto et al. 2017). In combination with the 9 values of inclination, this creates 36

variants of parameters for each galaxy. After generating each datacube realization, the resulting cubes were saved for extraction of the spectra.

During the creation of all variants of the model, each one was fitted to the observations, allowing amplitude scaling and shifting along the velocity axis. The first one is necessary since the flux of the model is not normalized, the latter because of possible misalignment due to the redshift uncertainty and rest-frame shifting.

The chi^2 values of all the realizations were then compared, and the model with the lowest value was considered to be the best-fitting model. We also did a visual inspection of all the observation-mock comparison plots, looking for possible problems with the representation of the observed line by the mock. For the majority of the galaxies, residuals defined as $res = obs - mock$ remain under 3σ threshold imposed by the RMS of observation, mainly in the wings of the lines. Few exceptions were present, possibly being evidence of massive non-circular motions in the galaxy we are looking for. Parameters of the best-fitting model are saved alongside the model parameters in a catalog, which can be seen in Appendix subsection A.3. The best-fitting model spectra were also saved into files containing their velocity-flux values.

3.4 Bringing out outflows

To allow us to probe fainter signals and to receive statistically driven results instead of results for individual galaxies, we split the sample into three bins according to stellar mass, and within each bin combined the spectra of the galaxies.

The stellar mass bins were chosen so that they roughly separate galaxies according to their expected outflow driving mechanisms. The first bin with $\log(M_*/M_\odot) \in [9.0, 10.0)$ corresponds to low-mass galaxies where star formation should be the dominant driver of outflows. On the other hand, the highest mass bin with $\log(M_*/M_\odot) \in [10.5, 11.5)$ represents massive galaxies, where the potential well of the galaxy is deep enough that the energy injected by the star formation activity is not sufficient and energy of AGN is needed to drive massive outflows. The middle bin with $\log(M_*/M_\odot) \in [10.0, 10.5)$ serves as a comparison sample since the galaxies within this range of stellar masses are expected to be the most efficient in converting material into stars, the likely reason being that the potential well becomes deep enough to suppress part of the star formation feedback while the central SMBH is mostly not active.

3.4.1 Stacking obs/mock spectra

Stacking was achieved by combining all spectra from the given mass bin and calculation of "5% trimmed mean" for each channel. It can be expressed as

$$f_{i,stack} = \text{trmean5}(\{f_i\}) \,, \tag{3.15}$$

where f_i is the flux of i-th channel and trmean5 represents a function, which removes 5 % of the highest and lowest values from the set of flux values of i-th channel of all the galaxies used for the stack $\{f_i\}$. Removing the ends of the set distribution makes it more robust regarding outliers while maintaining the sensitivity of the classical mean. While in

principle other statistical methods can be used to derive representative values, we chose this for the aforementioned reasons.

Each mass bin has been stacked individually and saved in a standardized velocity-flux format. An overview of the final stacks can be seen in Figure 3.6

3.5 Stack fitting

The last step in our method was the fitting of the observation stack with two models. First, it was only the stack of mocks, assuming the disc models can represent all the emission. The second model consists of the disc model with an added Gaussian component, included to represent the potential outflow.

Fitting was done with the same functions as in subsection 3.3.6 with the difference of omitting the possibility of velocity shift of the mock stack. To quantify the importance of the inclusion of Gaussian component, we calculate the reduced chi^2 and Bayesian information criterion (BIC) (Schwarz 1978, see also Liddle 2007) values for both fits according to the following formulas

$$chi^2_R = \frac{chi^2}{\nu} \,, \tag{3.16}$$

$$BIC = chi^2 + p \ln n \,, \tag{3.17}$$

where chi^2 is based on (3.13), $\nu = n - p$ is the degree of freedom, n is the number of flux points used for fit and p the number of parameters of the fit. The RMS of the observation stacks was calculated in extended velocity ranges $v \in [-1500, -600]\,\mathrm{km\,s^{-1}}$ and $v \in [600, 1500]\,\mathrm{km\,s^{-1}}$ compared to single observations.

Results of our analysis are discussed in the following chapter 4.

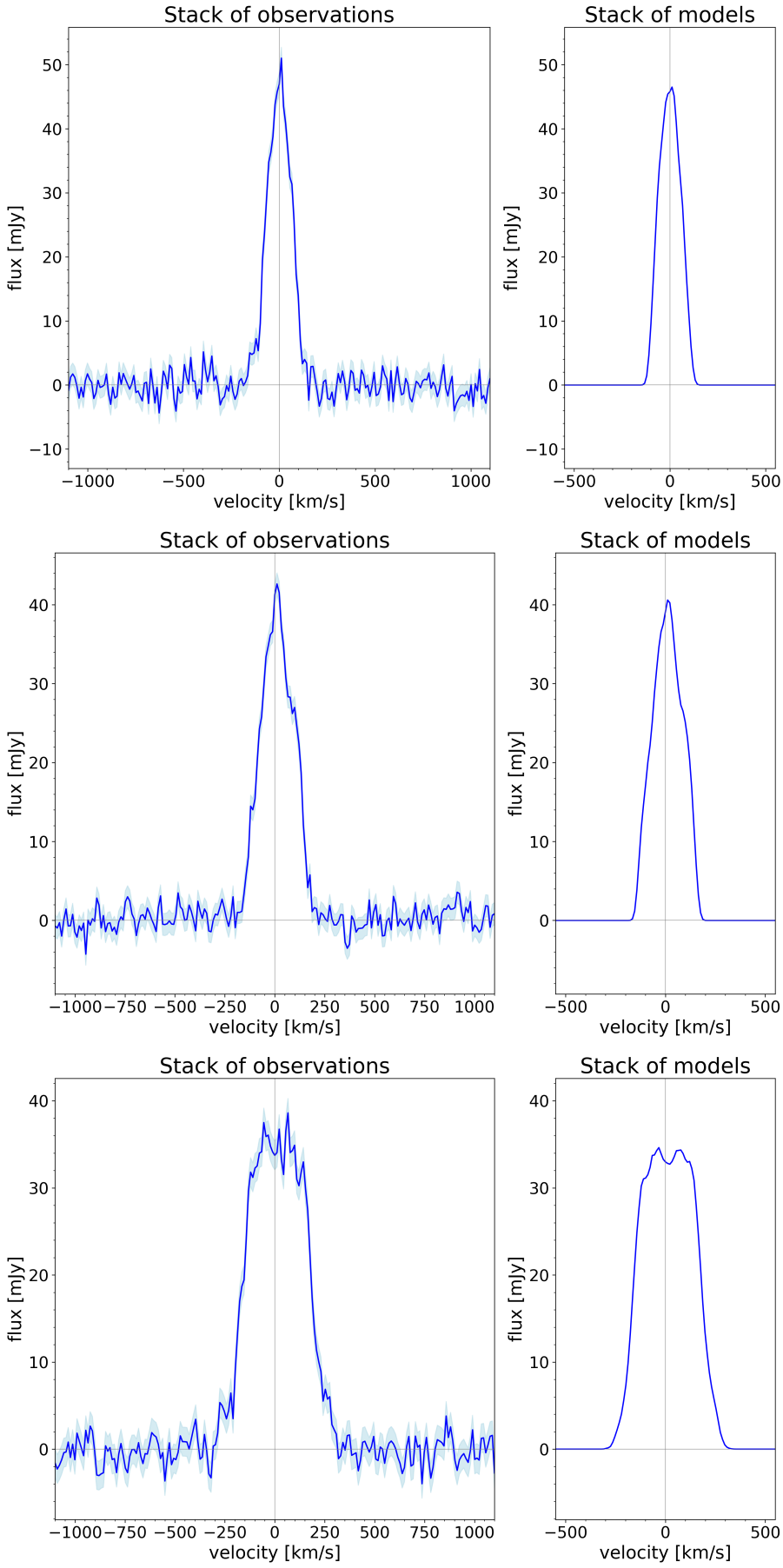

Figure 3.6: Overview of the stacks - observations (left) and mocks (right) - for different mass bins.

Chapter 4

Results

Our analysis aims to look for evidence of the presence of massive molecular gas outflows in local galaxies and explore possible connections to the stellar mass of the host galaxies. To achieve this goal, we used the methodology described in chapter 3 to derive three stacks of observed spectra and three stacks of mock spectra of galaxies in mass bins $\log(M_*/M_\odot) = [9.0, 10.0)$, $[10.0, 10.5)$ and $[10.5, 11.5)$. The first mass bin represents galaxies where star formation poses as the dominant driving force of outflows with the highest mass bin representing galaxies where energetic AGNs are needed to expel the gas from deep potential wells of galaxies. The middle mass bin serves as a comparison sample, representing the transition between the two regions of dominance of the two driving engines.

The presence of outflows is expected to create an excess emission in the observations, which is not representable by our disc model, thus bringing the need for a second component. We introduce a Gaussian profile to model this second component, creating the disc+Gaussian set of models. Each observation stack was fitted with the two models, disc-only and disc+Gaussian, to study the difference between the observed and mock stacks for a given mass bin. To quantify the potential improvement of the disc+Gaussian model, we searched for changes in residuals, reduced chi^2 and BIC (Schwarz 1978, see also Liddle 2007) as compared with values obtained with the disc-only fit. We consider the disc+Gaussian model to be necessary (as opposed to the disc-only model) only if the residuals of the disc-only fit are above 3σ limit imposed by the RMS of observations stack, $\Delta chi^2_R \geq RMS$ and $\Delta BIC > 10$[1]. Stacks of observations with corresponding fits with both the disc-only and disc+Gaussian models for the three stellar mass bins are shown in Figure 4.1 and the values of chi^2_R and BIC for all fits are also reported in Table 4.1.

The figure Figure 4.1a shows the stacked spectra (blue curves) for galaxies with $\log(M_*/M_\odot) \in [9.0, 10.0)$ with the disc-only fit in the upper panel and disc+Gaussian model fit in the lower panel. The residuals defined as $res = f_{obs} - f_{model}$ are shown below the figures, allowing us to assess the quality of the fit channel by channel. As can be seen, the disc-only model can reproduce the data within the 3σ error (dashed line) imposed by $RMS_{obs} = \sigma$ (dotted line). This is statistically confirmed by the χ^2_R value being consistent with unity within the error imposed by the RMS of the noise of the stacked spectrum (1σ dotted line, 3σ dashed line). The addition of a Gaussian component does not provide

[1] Fabozzi et al. 2014 shows this criterion as strong support for candidate model

any significant improvement, as indicated by the negligible change of residuals together with Δchi^2_R between the two models being insignificant compared to the *RMS* of the noise. $\Delta BIC > 10$ favors the disc+Gaussian model, but being the only indicator of such improvement it is not enough to rule out the disc-only model, as several factors, e.g. the nature of the models, can lead to a shift of the "critical" value.

The middle mass bin, shown in the Figure 4.1b, represents galaxies with $\log(M_*/M_\odot) \in [10.0, 10.5)$. The residuals of the disc-only model are under 3σ and the $chi^2_R = 1.03$. This shows a perfect match between the observations and the disc-only model. The preference for the disc-only model is further supported by the increase of *BIC* for the disc+Gaussian model and the very low change $\Delta chi^2_R = 0.05$.

The highest mass bin, galaxies with $\log(M_*/M_\odot) \in [10.5, 11.5)$, is presented in the Figure 4.1c. The results for this bin are similar to the low-mass bin. The observations are well reproduced by the disc-only model, as demonstrated by the residuals and $chi^2_R = 0.92$. The addition of the Gaussian component leads to a non-substantial improvement, as indicated by the low $\Delta chi^2_R = 0.06$ and $\Delta BIC = 2.03$.

Our results indicate that generally most of the CO(1-0) originates from the molecular disc of galaxies, without strong evidence of ubiquitous large-scale molecular outflows, as predicted by Nelson et al. 2019. Our findings are consistent with other studies focused on the search for large-scale outflows in local galaxies (e.g Concas et al. 2017), where only galaxies undergoing either a starburst event or galaxies with active AGN are observed to produce massive outflows (e.g. McQuinn et al. 2019, Perna et al. 2019, Marasco et al. 2020, Fluetsch et al. 2021).

fit components	chi^2_R	*BIC*	Δchi^2_R	ΔBIC
Disc only	1.35	374.05	–	–
Disc + Gaussian	1.24	357.11	0.11	16.94

(a) $9.0 \leq \log(M_*/M_\odot) < 10.0$, $RMS = 1.69$

fit components	chi^2_R	*BIC*	Δchi^2_R	ΔBIC
Disc only	1.03	285.2	–	–
Disc + Gaussian	0.98	285.78	0.05	-0.58

(b) $10.0 \leq \log(M_*/M_\odot) < 10.5$, $RMS = 1.4$

fit components	chi^2_R	*BIC*	Δchi^2_R	ΔBIC
Disc only	0.92	254.53	–	–
Disc + Gaussian	0.86	252.5	0.06	2.03

(c) $10.5 \leq \log(M_*/M_\odot) < 11.5$, $RMS = 1.66$

Table 4.1: Results of fitting the observations stack of each mass bin with mock only and mock+gaussian model

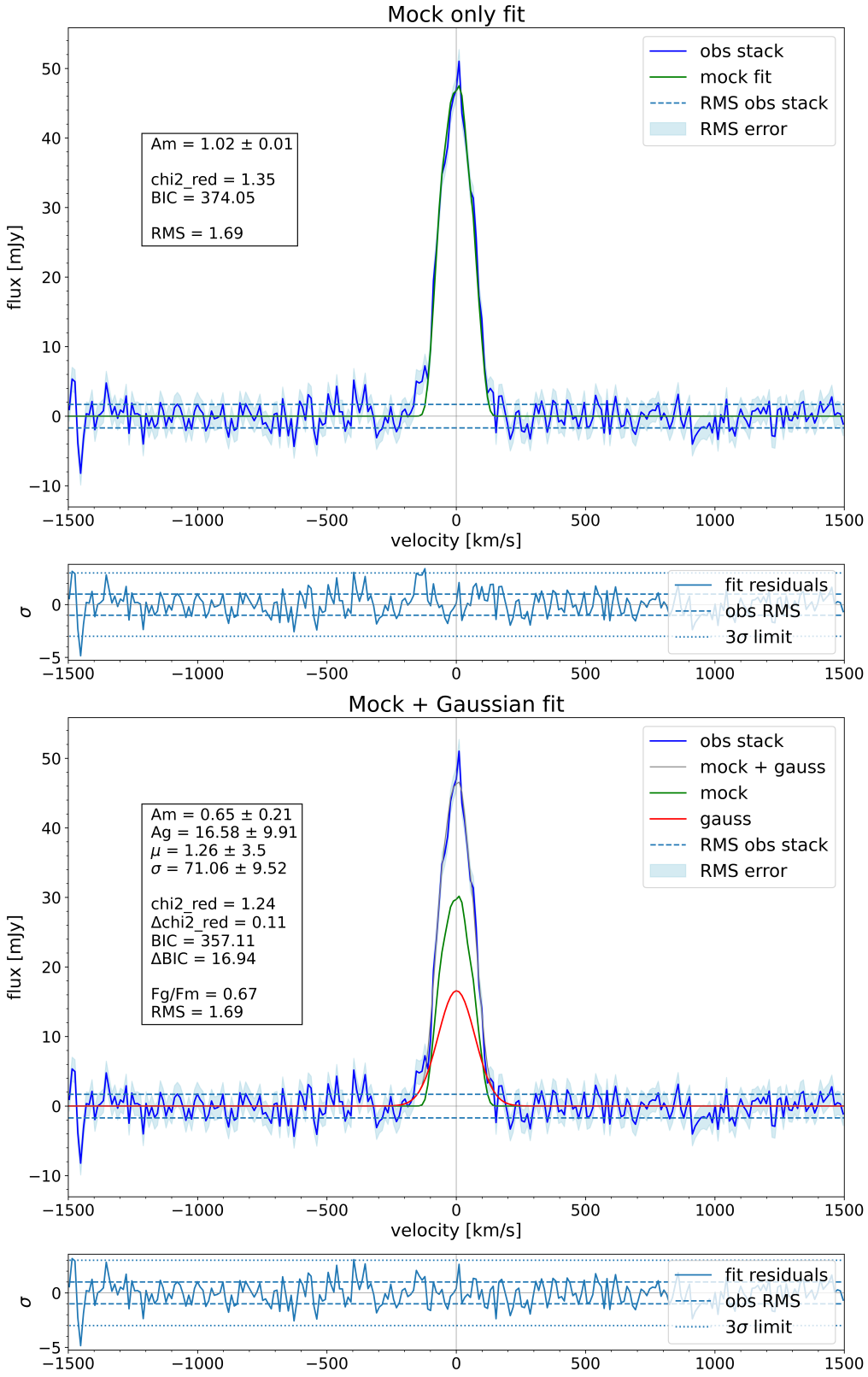

(a) Stack of galaxies with $\log(M_*/M_\odot) \in [9.0, 10.0)$

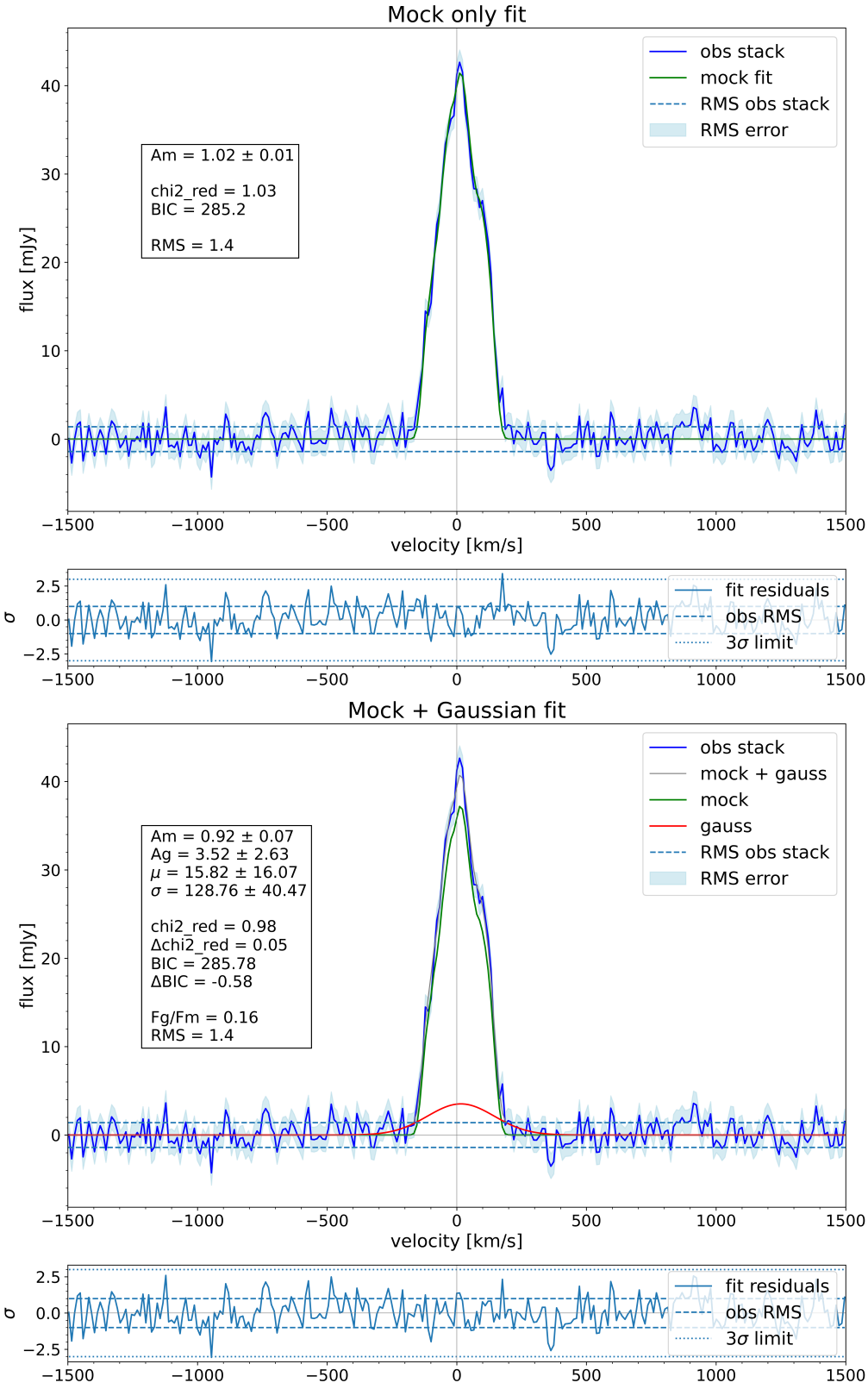

(b) Stack of galaxies with $\log(M_*/M_\odot) \in [10.0, 10.5)$

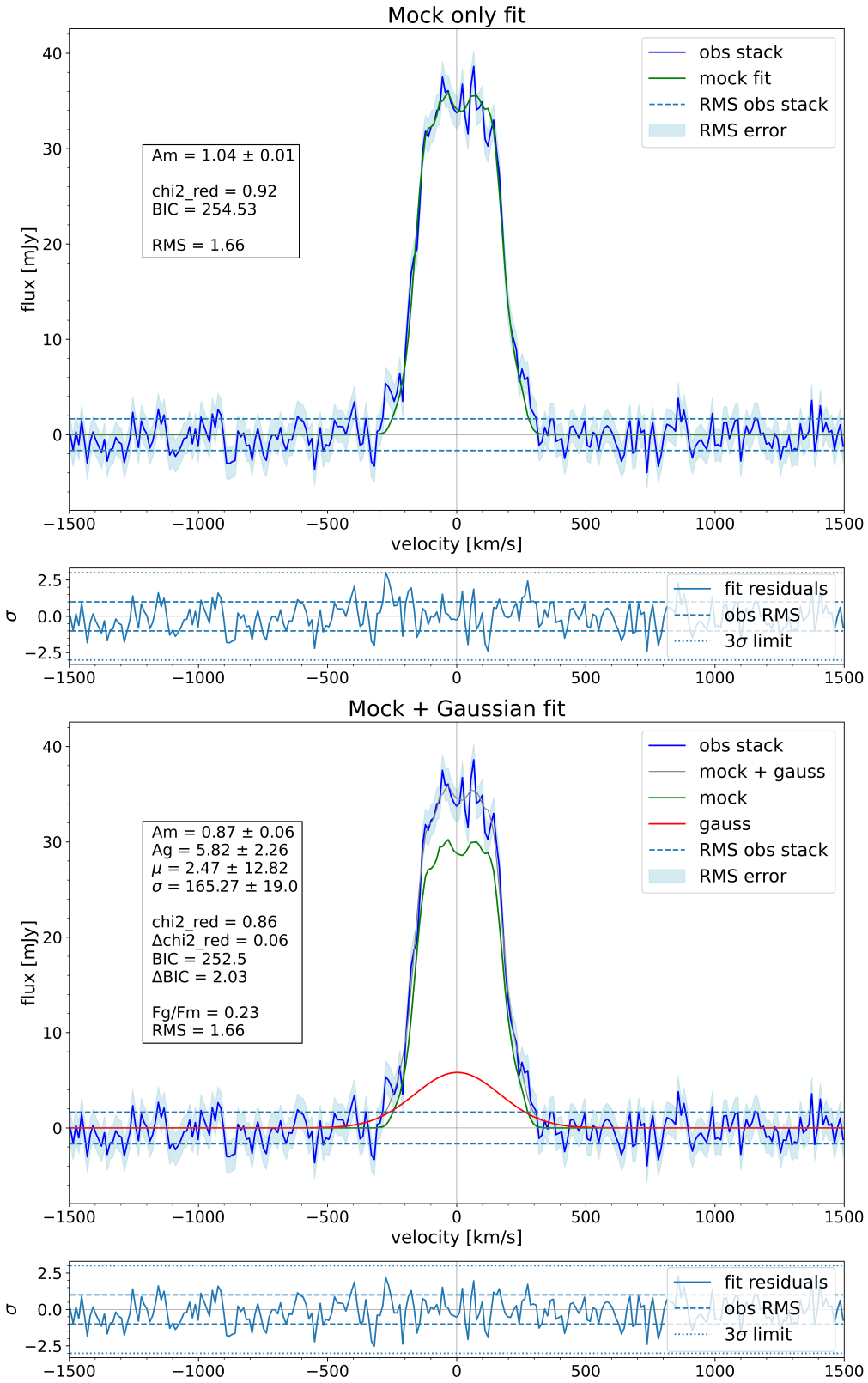

(c) Stack of galaxies with $\log(M_*/M_\odot) \in [10.5, 11.5)$

Figure 4.1: The stacks of observations (blue line) for given mass bins with disc-only (left column) and disc+Gaussian (right column) model fits (green lines). The dotted horizontal line represents the *RMS* quantified in the $v \in [-1500, -600]\,\mathrm{km\,s^{-1}}$ and $v \in [600, 1500]\,\mathrm{km\,s^{-1}}$. Each stack-fit plot is accompanied by the residuals plot, defined as $res = f_{obs} - f_{model}$ with the $\sigma = RMS$ (dotted) and 3σ (dashed) lines.

Conclusions

Galactic outflows are a prominent part of state-of-the-art ΛCDM cosmological simulations, presenting a mechanism allowing them to reproduce the observed parameters of galaxies, e.g. the galaxy stellar mass function. The observational picture of these phenomena is still incomplete, presenting a challenge while interpreting the results and assessing the precision of simulations.

In this thesis we look for evidence for the presence of large-scale molecular phase outflows in local galaxies, suggested by simulations (e.g. Nelson et al. 2019), utilizing CO(1-0) observations carried out under the xCOLD GASS survey (Saintonge et al. 2017). From the 532 galaxies covered by the survey, we use the observed spectra of 236 objects, providing a representative unbiased sample of local galaxies with $\log(M_*/M_\odot) \in [9.0, 11.5)$, selected based on the quality of their spectra (see section 2.3). These objects are further divided into 3 mass bins with $\log(M_*/M_\odot) \in [9.0, 10.0)$, representing low mass galaxies where the main driving mechanism behind outflows is thought to be star formation activity (e.g. Hopkins et al. 2014), $\log(M_*/M_\odot) \in [10.5, 11.5)$ where AGN or extremely strong starburst events are needed to supply the interstellar medium with enough energy to create outflows (e.g. King et al. 2015), and $\log(M_*/M_\odot) \in [10.0, 10.5)$ being a comparison group, where the efficiency of both mechanisms to create outflows is the most limited. For analysis, we use the physically motivated disc-decomposition technique and stacking of spectra, proposed by Concas et al. 2022 to search for evidence of the molecular outflows.

Our results show no evidence for massive-scale molecular outflows being ubiquitous in local galaxies. This result is consistent with the findings from other studies focused on the search for large-scale outflows in local galaxies (e.g. Concas et al. 2017), where only galaxies undergoing either a starburst event or galaxies with active AGN are observed to produce massive outflows (e.g. McQuinn et al. 2019, Perna et al. 2019, Marasco et al. 2020, Fluetsch et al. 2021). This is however in direct contradiction with the predictions from the latest cosmological simulations, e.g. Nelson et al. 2019, which predict their large-scale and ubiquitous presence.

We do not claim that outflows with low flux or low velocity cannot be hidden below our detection limit. Single galaxies with large-scale molecular outflows are observed (e.g. McQuinn et al. 2019, Fluetsch et al. 2021), but their possible contributions are not representative of the overall population. Our results are based on the exponential disc distribution model and the assumption that the free values of *inc* and r_{SB} used to find the best-fit mock are realistic. In future work, we will characterize the detection limits for our stacked spectra and explore the impact of the assumptions used to create and identify the best-fit mock. Deeper spectroscopic observations of the molecular gas are needed to quantify the real extent of the outflows in the local population of galaxies.

Bibliography

Bacchini, Cecilia et al. (Sept. 2020). "Evidence for supernova feedback sustaining gas turbulence in nearby star-forming galaxies". In: 641, A70, A70. DOI: 10.1051/0004-6361/202038223. arXiv: 2006.10764 [astro-ph.GA].

Bolatto, Alberto D. et al. (Sept. 2017). "The EDGE-CALIFA Survey: Interferometric Observations of 126 Galaxies with CARMA". In: 846.2, 159, p. 159. DOI: 10.3847/1538-4357/aa86aa. arXiv: 1704.02504 [astro-ph.GA].

Bovy, Jo (Feb. 2015). "galpy: A python Library for Galactic Dynamics". In: 216.2, 29, p. 29. DOI: 10.1088/0067-0049/216/2/29. arXiv: 1412.3451 [astro-ph.GA].

Catinella, Barbara et al. (May 2018). "xGASS: total cold gas scaling relations and molecular-to-atomic gas ratios of galaxies in the local Universe". In: 476.1, pp. 875–895. DOI: 10.1093/mnras/sty089. arXiv: 1802.02373 [astro-ph.GA].

Chiang, I-Da et al. (Mar. 2024). "Resolved Measurements of the CO-to-H_2 Conversion Factor in 37 Nearby Galaxies". In: 964.1, 18, p. 18. DOI: 10.3847/1538-4357/ad23ed. arXiv: 2311.00407 [astro-ph.GA].

Concas, A. et al. (Oct. 2017). "Light breeze in the local Universe". In: 606, A36, A36. DOI: 10.1051/0004-6361/201629519. arXiv: 1701.06569 [astro-ph.GA].

Concas, Alice et al. (June 2022). "Being KLEVER at cosmic noon: Ionized gas outflows are inconspicuous in low-mass star-forming galaxies but prominent in massive AGN hosts". In: 513.2, pp. 2535–2562. DOI: 10.1093/mnras/stac1026. arXiv: 2203.11958 [astro-ph.GA].

Davis, Timothy A. et al. (Feb. 2013). "The ATLAS^{3D} Project - XIV. The extent and kinematics of the molecular gas in early-type galaxies". In: 429.1, pp. 534–555. DOI: 10.1093/mnras/sts353. arXiv: 1211.1011 [astro-ph.CO].

de Vaucouleurs, Gerard (Jan. 1948). "Recherches sur les Nebuleuses Extragalactiques". In: *Annales d'Astrophysique* 11, p. 247.

Di Cintio, Arianna and Federico Lelli (Feb. 2016). "The mass discrepancy acceleration relation in a ΛCDM context". In: 456.1, pp. L127–L131. DOI: 10.1093/mnrasl/slv185. arXiv: 1511.06616 [astro-ph.GA].

Fabozzi, Frank et al. (Mar. 2014). "Appendix E: Model Selection Criterion: AIC and BIC". In: pp. 399–403. ISBN: 9781118573204. DOI: 10.1002/9781118856406.app5.

Fluetsch, A. et al. (Aug. 2021). "Properties of the multiphase outflows in local (ultra)luminous infrared galaxies". In: 505.4, pp. 5753–5783. DOI: 10.1093/mnras/stab1666. arXiv: 2006.13232 [astro-ph.GA].

Freeman, K. C. (June 1970). "On the Disks of Spiral and S0 Galaxies". In: 160, p. 811. DOI: 10.1086/150474.

Genzel, R. et al. (Nov. 2014). "Evidence for Wide-spread Active Galactic Nucleus-driven Outflows in the Most Massive z ~1-2 Star-forming Galaxies". In: 796.1, 7, p. 7. DOI: 10.1088/0004-637X/796/1/7. arXiv: 1406.0183 [astro-ph.GA].

Ginsburg, Adam et al. (Feb. 2019). *radio-astro-tools/spectral-cube: v0.4.4*. Version v0.4.4. DOI: 10.5281/zenodo.2573901.

Heckman, Timothy M., Lee Armus, and George K. Miley (Dec. 1990). "On the Nature and Implications of Starburst-driven Galactic Superwinds". In: 74, p. 833. DOI: 10.1086/191522.

Heckman, Timothy M. and Todd A. Thompson (2017). "Galactic Winds and the Role Played by Massive Stars". In: *Handbook of Supernovae*. Ed. by Athem W. Alsabti and Paul Murdin, p. 2431. DOI: 10.1007/978-3-319-21846-5_23.

Hernquist, Lars (June 1990). "An Analytical Model for Spherical Galaxies and Bulges". In: 356, p. 359. DOI: 10.1086/168845.

Hopkins, Philip F. et al. (Nov. 2014). "Galaxies on FIRE (Feedback In Realistic Environments): stellar feedback explains cosmologically inefficient star formation". In: 445.1, pp. 581–603. DOI: 10.1093/mnras/stu1738. arXiv: 1311.2073 [astro-ph.CO].

King, Andrew and Ken Pounds (Aug. 2015). "Powerful Outflows and Feedback from Active Galactic Nuclei". In: 53, pp. 115–154. DOI: 10.1146/annurev-astro-082214-122316. arXiv: 1503.05206 [astro-ph.GA].

Liddle, Andrew R. (May 2007). "Information criteria for astrophysical model selection". In: 377.1, pp. L74–L78. DOI: 10.1111/j.1745-3933.2007.00306.x. arXiv: astro-ph/0701113 [astro-ph].

Marasco, A. et al. (Dec. 2020). "Galaxy-scale ionised winds driven by ultra-fast outflows in two nearby quasars". In: 644, A15, A15. DOI: 10.1051/0004-6361/202038889. arXiv: 2009.11294 [astro-ph.GA].

McQuinn, Kristen. B. W., Liese van Zee, and Evan D. Skillman (Nov. 2019). "Galactic Winds in Low-mass Galaxies". In: 886.1, 74, p. 74. DOI: 10.3847/1538-4357/ab4c37. arXiv: 1910.04167 [astro-ph.GA].

Moster, Benjamin P., Thorsten Naab, and Simon D. M. White (Feb. 2013). "Galactic star formation and accretion histories from matching galaxies to dark matter haloes". In: 428.4, pp. 3121–3138. DOI: 10.1093/mnras/sts261. arXiv: 1205.5807 [astro-ph.CO].

Navarro, Julio F., Carlos S. Frenk, and Simon D. M. White (May 1996). "The Structure of Cold Dark Matter Halos". In: 462, p. 563. DOI: 10.1086/177173. arXiv: astro-ph/9508025 [astro-ph].

Nelson, Dylan et al. (Dec. 2019). "First results from the TNG50 simulation: galactic outflows driven by supernovae and black hole feedback". In: 490.3, pp. 3234–3261. DOI: 10.1093/mnras/stz2306. arXiv: 1902.05554 [astro-ph.GA].

Perna, M. et al. (Mar. 2019). "Multi-phase outflows in Mkn 848 observed with SDSS-MaNGA integral field spectroscopy". In: 623, A171, A171. DOI: 10.1051/0004-6361/201834193. arXiv: 1901.02027 [astro-ph.GA].

Popesso, P. et al. (Feb. 2023). "The main sequence of star-forming galaxies across cosmic times". In: 519.1, pp. 1526–1544. DOI: 10.1093/mnras/stac3214. arXiv: 2203.10487 [astro-ph.GA].

Saintonge, Amélie et al. (Dec. 2017). "xCOLD GASS: The Complete IRAM 30 m Legacy Survey of Molecular Gas for Galaxy Evolution Studies". In: 233.2, 22, p. 22. DOI: 10.3847/1538-4365/aa97e0. arXiv: 1710.02157 [astro-ph.GA].

Schwarz, Gideon (July 1978). "Estimating the Dimension of a Model". In: *Annals of Statistics* 6.2, pp. 461–464.

Sérsic, J. L. (Feb. 1963). "Influence of the atmospheric and instrumental dispersion on the brightness distribution in a galaxy". In: *Boletin de la Asociacion Argentina de Astronomia La Plata Argentina* 6, pp. 41–43.

Simard, Luc et al. (Sept. 2011). "A Catalog of Bulge+disk Decompositions and Updated Photometry for 1.12 Million Galaxies in the Sloan Digital Sky Survey". In: 196.1, 11, p. 11. DOI: 10.1088/0067-0049/196/1/11. arXiv: 1107.1518 [astro-ph.CO].

Springel, Volker, Carlos S. Frenk, and Simon D. M. White (Apr. 2006). "The large-scale structure of the Universe". In: 440.7088, pp. 1137–1144. DOI: 10.1038/nature04805. arXiv: astro-ph/0604561 [astro-ph].

Taylor, M. B. (Dec. 2005). "TOPCAT & STIL: Starlink Table/VOTable Processing Software". In: *Astronomical Data Analysis Software and Systems XIV*. Ed. by P. Shopbell, M. Britton, and R. Ebert. Vol. 347. Astronomical Society of the Pacific Conference Series, p. 29.

Tomisaka, Kohji and Satoru Ikeuchi (July 1988). "Starburst Nucleus: Galactic Scale Bipolar Flow". In: 330, p. 695. DOI: 10.1086/166505.

Appendix

A Galaxy sample parameters

A.1 Overview of our galaxy sample

Basic information about galaxies from our sample

Parameter	Unit	Description
id	—	xCOLD GAS survey id, Saintonge et al. 2017
$\log M_*$	$M_\odot$	logarithm of the stellar mass from Saintonge et al. 2017
lum. dist	Mpc	luminosity distance from Saintonge et al. 2017
z_{co}	—	redshift of the galaxy from Saintonge et al. 2017
RMS_{obs}	mJy	RMS of observed spectrum, as defined in section 3.2
S/N	—	signal-to-noise ratio as defined in section 3.2

id	SDSS	$\log M_*$	lum. dist	z_{CO}	RMS_{obs}	S/N
522	J112418.64+003837.4	10.08	115.22	0.026	19.3	4.1
947	J133647.92+010914.0	10.39	208.87	0.047	13.6	2.2
1115	J141814.91+005328.0	10.11	113.35	0.026	21.0	4.9
1137	J142314.68+005842.0	10.28	176.86	0.040	9.1	8.8
1221	J143525.34+002003.6	10.20	151.88	0.035	17.9	7.6
1977	J231815.66+001540.2	10.78	130.54	0.030	14.2	2.5
3261	J005532.61+154632.9	10.08	165.07	0.037	10.6	3.7
3504	J011823.44+133728.4	10.16	167.52	0.038	9.8	4.5
3524	J011716.09+143720.5	10.73	167.65	0.038	5.7	1.6
3819	J014143.18+134032.8	10.67	200.76	0.045	12.9	6.4
3962	J020359.14+141837.3	10.90	189.02	0.043	10.8	7.1
3981	J021404.39+131156.3	10.55	183.82	0.042	6.6	2.1
4017	J020517.54+133020.6	10.23	112.77	0.026	10.7	2.2
4030	J020939.47+135859.4	11.33	218.33	0.049	15.0	2.2
4041	J021136.94+143045.2	10.41	114.64	0.026	10.3	2.5
4048	J021219.38+133645.6	10.55	182.82	0.041	6.9	2.7
4216	J015551.98+145624.9	10.74	193.99	0.044	14.1	6.1
4230	J015709.80+143259.5	11.01	115.40	0.026	7.4	2.2
5442	J110032.51+020657.8	11.10	173.78	0.039	13.2	2.9

id	SDSS	logM$_*$	lum. dist	z$_{CO}$	RMS$_{obs}$	S/N
6506	J124309.36+033452.2	10.77	216.17	0.049	11.3	3.0
6749	J130750.80+031140.7	11.12	169.97	0.039	6.8	2.6
7493	J142720.13+025018.1	10.56	115.53	0.026	15.9	4.2
8349	J093953.62+034850.2	10.37	124.82	0.029	8.8	2.9
8724	J102231.19+043456.7	10.87	125.04	0.029	16.0	2.2
8914	J104402.21+043946.8	10.42	116.29	0.027	16.0	2.5
8945	J105315.29+042003.1	10.83	184.23	0.041	9.8	2.0
9483	J142056.54+035217.4	10.71	155.76	0.035	12.1	3.8
9551	J142732.37+044917.8	10.91	117.50	0.027	18.6	5.5
9704	J144059.30+030813.5	10.95	115.98	0.027	9.4	2.2
9814	J143348.34+035724.7	10.87	128.13	0.029	16.5	3.1
10019	J145153.39+032147.7	10.68	134.89	0.031	13.6	2.8
10218	J151140.36+034034.2	10.76	205.61	0.046	14.2	2.8
10841	J221111.69+114802.6	10.36	118.16	0.027	5.6	2.3
10850	J220538.79+122521.3	10.28	156.17	0.036	7.8	1.7
10943	J221540.59+133616.9	10.23	120.44	0.028	11.1	1.5
10952	J221657.95+133235.0	10.47	114.42	0.026	9.8	1.6
11019	J223810.59+142626.1	10.05	158.38	0.036	10.9	2.2
11071	J225726.69+130005.9	10.56	112.15	0.026	9.9	1.7
11112	J230240.30+131944.6	10.82	120.93	0.028	13.1	6.5
11120	J230343.06+135535.5	10.41	118.30	0.027	12.1	1.8
11223	J230616.43+135856.3	10.64	156.35	0.036	7.3	10.2
11270	J231816.95+133426.6	10.07	174.37	0.040	7.8	1.6
11295	J231334.71+135912.3	11.09	175.64	0.040	8.1	1.9
11298	J231330.39+140350.0	10.10	173.96	0.039	7.4	1.8
11311	J231229.22+135632.1	10.92	149.94	0.034	10.6	2.7
11340	J231316.47+145415.6	10.10	157.39	0.036	8.9	4.0
11349	J231836.21+151758.7	10.13	111.84	0.026	13.9	3.0
11408	J232227.40+134857.1	10.05	113.57	0.026	14.6	5.7
11845	J235644.47+135435.4	10.60	159.92	0.036	14.3	3.5
12371	J111306.40+051403.0	10.80	191.02	0.043	11.3	1.6
12533	J113116.03+043908.7	10.09	145.35	0.033	13.7	7.6
13005	J125125.64+035159.5	10.28	216.35	0.049	12.3	3.4
13074	J125134.48+055148.8	10.85	215.89	0.049	12.9	2.1
13624	J135152.41+032718.0	10.31	129.78	0.030	16.1	3.3
13666	J140008.99+040450.8	10.18	178.64	0.040	10.1	3.9
14712	J091858.06+055318.2	10.55	168.70	0.038	16.6	7.7
14831	J100530.26+054019.4	11.21	196.55	0.044	12.5	1.8
15151	J104251.39+055135.5	10.99	146.88	0.033	7.2	3.8
15155	J104054.93+055930.8	10.19	121.29	0.027	12.6	5.2
15181	J104002.96+060114.0	11.18	207.81	0.047	7.3	2.3
16655	J090439.54+053043.3	10.63	146.61	0.033	7.7	2.1
16695	J090115.64+040705.1	10.07	123.12	0.028	10.1	1.6
16841	J093136.49+065708.6	10.06	139.69	0.032	11.1	3.3

id	SDSS	$\log M_*$	lum. dist	z_{CO}	RMS_{obs}	S/N
17135	J080741.39+255531.0	10.53	208.87	0.047	11.1	1.9
17865	J112920.69+083608.3	10.28	117.94	0.027	12.1	2.6
18421	J122006.47+100429.2	10.60	191.89	0.043	10.9	2.0
18469	J123251.49+084423.9	10.15	148.41	0.034	9.5	2.2
18673	J095301.79+072736.4	10.38	169.87	0.038	13.4	2.9
18686	J095302.62+075029.3	10.55	181.41	0.041	9.4	2.4
18702	J095051.58+081340.7	10.20	130.86	0.030	8.0	2.2
18887	J102055.54+081849.4	10.76	203.00	0.046	5.6	1.8
19918	J083846.98+072850.5	10.82	205.02	0.046	7.0	1.7
19949	J090011.06+074333.9	10.69	126.34	0.029	14.5	3.7
20133	J093236.58+095025.9	10.86	217.23	0.049	11.2	1.8
20286	J095439.45+092640.7	10.53	151.93	0.035	13.3	1.8
22822	J095144.91+353719.6	10.56	117.99	0.027	16.0	2.9
22999	J102316.42+115120.4	10.64	201.49	0.045	15.8	2.9
23026	J102721.97+110447.9	11.16	141.94	0.032	10.7	2.3
23088	J102636.10+120224.7	10.62	137.62	0.031	11.7	3.2
23245	J104339.07+120338.3	10.11	114.60	0.026	17.3	2.7
23320	J104329.94+120515.8	10.12	116.38	0.027	10.0	2.3
23419	J105118.51+124523.4	10.39	176.41	0.040	11.8	2.6
23453	J105800.29+115913.6	10.13	153.06	0.034	9.6	1.7
23577	J110949.30+124617.3	10.44	188.38	0.043	16.8	3.3
23685	J112311.63+130703.7	10.70	208.32	0.047	11.4	2.5
24183	J121744.10+131015.7	10.77	189.56	0.043	13.8	4.1
24426	J123622.72+133610.3	10.13	133.81	0.031	9.4	3.2
24496	J111809.91+074653.9	10.60	185.92	0.042	8.5	3.6
24973	J143518.37+350707.2	10.61	124.73	0.029	16.4	29.1
25448	J133003.89+121030.6	10.68	198.01	0.045	9.8	1.8
25752	J090124.57+101200.6	10.56	161.86	0.037	13.0	5.3
25763	J090311.24+100907.1	10.11	129.74	0.030	15.9	5.8
26040	J095337.10+120745.3	10.01	132.60	0.030	7.2	2.0
26056	J095007.20+124446.0	10.12	129.74	0.030	9.9	2.2
26221	J101638.39+123438.5	10.99	138.88	0.032	7.4	11.9
26368	J101941.29+125034.7	10.27	144.41	0.033	11.5	2.4
26570	J103905.90+132153.5	10.00	142.43	0.032	5.5	3.4
26598	J103349.98+125242.0	10.47	110.06	0.025	12.6	2.7
26639	J104046.05+134659.9	10.24	139.24	0.032	9.2	1.7
26822	J125129.06+134654.5	11.03	165.48	0.038	11.9	3.7
26958	J154654.33+055328.3	11.26	185.10	0.042	9.0	4.7
28168	J124054.96+080323.2	10.18	212.31	0.048	7.2	1.7
28365	J154122.58+281347.1	10.36	140.81	0.032	16.3	7.8
29624	J110050.33+133551.4	10.32	149.40	0.034	13.9	2.4
29842	J112131.76+132535.7	10.80	149.76	0.034	15.2	2.3
29871	J113212.42+132932.8	10.17	150.53	0.034	7.1	2.4
30332	J122312.26+142320.2	10.49	187.79	0.042	12.8	4.6

id	SDSS	logM$_*$	lum. dist	z$_{CO}$	RMS$_{obs}$	S/N
30439	J123410.30+155805.5	11.05	204.33	0.046	13.9	4.1
31188	J140312.00+344104.5	10.01	195.64	0.044	9.3	2.2
32257	J082944.36+222527.8	10.20	109.12	0.025	14.5	5.0
32308	J083934.43+252837.6	10.02	127.95	0.029	9.7	2.9
32568	J085857.78+285406.0	10.36	188.10	0.042	6.6	4.7
32619	J090459.97+282051.8	10.01	216.03	0.048	5.0	3.0
38462	J141545.94+102619.8	10.75	112.64	0.026	16.2	2.7
39119	J150926.10+101718.3	10.18	120.84	0.028	13.5	2.9
39270	J151220.62+092059.7	10.14	151.66	0.035	10.0	2.4
39548	J152522.51+094352.3	10.42	152.47	0.035	11.8	2.6
39595	J152716.72+100240.2	10.87	192.62	0.044	10.1	2.6
40439	J130415.04+091324.4	10.95	153.96	0.035	14.5	4.8
40781	J131934.30+102717.5	11.10	213.27	0.048	10.2	2.0
41728	J144434.33+085613.5	10.18	122.00	0.028	9.9	2.0
41783	J145730.93+082326.3	11.09	163.17	0.037	8.1	1.9
41969	J151531.54+062213.3	10.42	154.27	0.035	17.8	5.4
42013	J151604.47+065051.4	10.77	162.09	0.037	14.8	6.4
44710	J135156.88+291844.6	10.16	156.35	0.036	7.6	2.4
44718	J135034.46+292222.4	10.45	168.74	0.038	10.5	6.5
44942	J140205.90+260339.1	10.44	144.59	0.033	17.8	3.0
47221	J154902.67+175625.5	10.54	139.42	0.032	11.2	1.8
50550	J124128.01+284728.3	10.29	154.00	0.035	16.8	2.2
51161	J132522.77+271456.7	10.15	151.57	0.035	14.0	2.5
51276	J075404.48+135714.7	10.37	129.65	0.030	11.1	3.5
51563	J080442.30+154632.6	10.48	128.22	0.029	14.2	2.1
55541	J103246.99+211256.3	10.62	189.61	0.043	12.3	3.0
56304	J080534.10+102336.2	10.89	149.27	0.034	10.0	1.6
56312	J080456.34+102621.0	10.10	151.03	0.034	10.0	2.0
56375	J075719.71+111221.8	10.84	205.75	0.046	14.6	2.5
56632	J090437.07+133314.7	11.00	122.76	0.028	6.5	4.3
56662	J090254.93+133938.5	10.25	130.95	0.030	8.6	2.9
57017	J092229.28+142743.3	10.54	141.85	0.032	6.3	2.1
101004	J012130.66+143017.9	9.92	60.76	0.014	12.4	4.3
101007	J012109.32+154140.9	9.45	74.25	0.017	10.0	2.4
101025	J011437.36+011053.4	9.84	66.93	0.015	28.9	4.4
101037	J013737.13+000224.7	9.31	71.13	0.016	9.6	1.7
108016	J083356.65+265821.5	9.57	50.78	0.012	21.6	4.2
108021	J085518.73+272046.2	9.64	75.05	0.017	17.1	3.7
108026	J083203.49+240039.2	9.84	79.55	0.018	20.8	6.6
108045	J081905.10+214729.0	10.08	65.03	0.015	17.3	10.4
108050	J081919.78+210331.8	9.75	70.09	0.016	18.6	2.8
108051	J085603.97+132519.2	9.11	60.41	0.014	11.1	2.1
108054	J085949.04+050339.0	9.93	53.91	0.013	24.5	2.9
108064	J082607.43+212724.1	9.56	64.84	0.015	10.8	2.8

id	SDSS	$\log M_*$	lum. dist	z_{CO}	RMS_{obs}	S/N
108072	J081932.11+212339.4	9.98	59.06	0.014	22.1	3.0
108093	J083530.18+234034.3	9.94	72.74	0.017	18.6	3.6
108094	J084256.38+133829.6	9.68	72.92	0.017	25.4	8.4
108106	J081006.99+183818.0	9.85	70.52	0.016	30.6	6.6
108113	J081825.78+295734.3	9.88	86.56	0.020	10.5	2.7
108142	J081915.85+191847.6	9.61	82.47	0.019	8.4	1.7
108147	J081523.41+284407.2	9.64	85.81	0.020	11.7	1.9
109010	J093402.71+092845.1	9.75	43.89	0.010	25.7	2.8
109011	J094535.44+042438.1	9.51	86.61	0.020	9.6	1.5
109028	J092728.80+035546.5	10.07	77.20	0.018	22.4	3.3
109038	J090316.49+181539.8	9.21	49.91	0.012	13.4	1.9
109045	J092515.42+105312.1	9.86	51.75	0.012	12.7	3.2
109050	J095836.22+131519.0	9.26	50.39	0.012	9.8	2.5
109058	J095203.79+193904.0	9.91	69.90	0.016	18.5	2.0
109072	J094031.83+285809.5	9.68	81.98	0.019	11.2	2.0
109081	J095642.48+153811.2	9.22	65.95	0.015	15.6	2.6
109088	J095853.32+152247.7	9.52	67.26	0.015	13.2	1.5
109092	J093802.63+273923.5	9.70	77.96	0.018	13.2	1.8
109100	J094631.02+155310.7	9.51	54.85	0.013	12.2	1.6
109102	J092115.44+030904.0	9.38	50.74	0.012	9.0	1.5
109106	J095351.47+133654.4	9.65	70.48	0.016	14.6	3.4
109108	J094419.42+095905.1	9.62	44.09	0.010	30.1	2.9
109112	J092608.29+345343.4	9.46	71.06	0.016	12.2	2.4
109126	J093459.07+254932.3	9.14	56.98	0.013	13.0	4.0
109139	J091639.78+071559.0	9.59	81.48	0.019	14.9	1.7
110013	J101712.71+131131.3	9.71	75.89	0.017	25.2	1.7
110017	J103539.30+283356.8	9.85	63.74	0.015	22.0	3.7
110038	J100216.28+191256.3	10.00	71.90	0.017	15.8	2.4
110040	J102508.93+133605.1	9.83	80.82	0.019	17.5	2.9
110041	J103939.03+251921.8	9.93	75.23	0.017	23.6	4.4
110054	J104402.45+221527.1	9.75	85.28	0.020	10.4	2.6
110059	J103913.14+310650.4	9.41	82.23	0.019	4.9	1.7
110063	J105512.61+055145.3	9.17	50.35	0.012	9.4	2.3
110080	J101837.31+031548.9	9.20	62.52	0.014	9.5	2.8
111027	J115726.68+251359.0	9.37	64.59	0.015	11.7	2.3
111035	J111045.21+120058.1	9.75	46.58	0.011	19.3	3.1
111063	J115825.42+250551.5	9.61	60.97	0.014	12.3	2.9
111067	J112938.20+095803.3	9.27	85.52	0.020	5.7	2.2
111079	J113701.88+153414.0	9.88	57.33	0.013	17.7	3.3
111086	J113914.73+145932.5	9.64	61.83	0.014	11.8	2.3
111088	J115417.76+325139.5	9.31	45.94	0.011	13.0	2.0
111091	J115458.53+261209.0	9.70	74.47	0.017	16.0	2.6
112035	J125905.29+273839.8	9.67	78.71	0.018	15.9	6.9
112050	J124841.02+342839.3	9.42	61.38	0.014	13.6	2.9

id	SDSS	logM$_*$	lum. dist	z$_{CO}$	RMS$_{obs}$	S/N
112068	J120409.74+014933.4	9.67	74.54	0.017	20.8	1.7
112090	J120222.52+295142.3	9.98	44.97	0.011	21.1	13.4
112112	J122540.14+203142.4	9.92	79.43	0.018	23.1	2.3
112116	J125606.09+274041.1	9.12	71.49	0.016	12.0	3.5
113008	J135655.41+140832.0	9.31	65.08	0.015	11.3	2.0
113062	J132134.91+261816.7	9.91	71.64	0.017	22.6	3.9
113067	J135804.69+151853.4	9.89	81.17	0.019	19.2	2.7
113098	J131335.27+290735.4	9.86	86.94	0.020	14.8	2.2
113100	J130035.67+273427.2	9.89	73.74	0.017	19.8	3.6
113118	J133829.70+305912.8	9.12	69.21	0.016	7.1	1.9
113122	J135845.41+203942.6	9.89	69.95	0.016	30.9	2.1
113124	J132251.07+314934.3	9.41	77.38	0.018	8.7	1.6
113136	J134701.25+335336.9	9.78	71.74	0.017	13.3	2.4
113141	J131131.65+084435.5	9.54	57.67	0.013	18.6	2.2
113150	J135838.59+071259.4	9.93	63.33	0.015	17.9	2.5
114010	J142846.66+271502.4	9.71	63.83	0.015	11.8	1.7
114048	J142855.80+254415.4	9.97	68.84	0.016	10.7	1.8
114113	J140309.85+121013.4	9.07	74.29	0.017	6.8	2.0
114115	J140832.78+030127.5	9.65	76.10	0.018	11.0	2.6
114121	J142049.04+255731.7	9.77	64.50	0.015	14.4	2.7
114136	J142729.01+295707.2	9.24	63.07	0.015	12.6	2.2
114141	J140043.62+315338.0	9.45	63.39	0.015	12.9	1.6
114144	J142835.88+254231.7	9.86	58.67	0.014	18.7	7.7
122002	J224110.65+132023.6	9.47	75.24	0.017	8.6	2.0
122006	J225258.56+010833.8	9.50	71.34	0.017	7.7	2.6
123006	J231347.06+134115.3	9.84	66.53	0.015	15.0	5.3
123010	J231736.39+140004.3	9.94	63.72	0.015	19.0	15.2
124004	J002534.40+005048.7	9.31	77.42	0.018	15.7	1.9
124006	J001947.33+003526.7	9.75	76.84	0.018	11.7	2.7
124010	J002359.39+154613.5	9.93	76.87	0.018	23.0	5.3
124012	J000629.28+141056.5	9.74	77.11	0.018	13.4	2.1

A.2 Velocity profile parameters

Parameter	Unit	Description
id	—	xCOLD GAS survey id, Saintonge et al. 2017
scale	arcsec kpc^{-1}	angular scale used to convert physical to angular, see Table 3.2
r_{disc}	arcsec	scaling radius of stellar disc, as defined in Table 3.2
$\log M_{disc}$	$M_\odot$	logarithm of the mass of the stellar disc, see Table 3.2
$r_{1/4,bulge}$	arcsec	scaling radius of stellar disc, as defined in Table 3.2
$\log M_{bulge}$	$M_\odot$	logarithm of the mass of the stellar bulge, see Table 3.2
$\log M_{gas}$	$M_\odot$	logarithm of the mass of the gas disc, see Table 3.2
$\log M_{DMH}$	$M_\odot$	logarithm of the mass of the dark matter halo, see Table 3.2

id	scale	r_{disc}	$\log M_{disc}$	$r_{1/4,bulge}$	$\log M_{bulge}$	$\log M_{gas}$	$\log M_{DMH}$
522	0.53	6.72	9.95	3.32	9.48	9.69	11.55
947	0.92	4.22	10.33	1.40	9.47	9.83	11.81
1115	0.52	7.32	10.02	2.48	9.37	9.70	11.57
1137	0.79	5.62	10.26	0.95	8.88	9.78	11.70
1221	0.69	2.24	10.17	0.54	9.11	9.74	11.64
1977	0.60	12.08	10.49	2.59	10.47	10.00	12.49
3261	0.74	1.96	9.99	1.37	9.33	10.12	11.55
3504	0.75	6.11	10.10	3.05	9.27	9.83	11.61
3524	0.76	2.32	10.54	0.81	10.29	9.64	12.37
3819	0.89	1.55	10.67	0.00	0.00	10.27	12.24
3962	0.84	6.19	10.70	1.70	10.48	10.17	12.79
3981	0.82	3.72	10.40	1.29	10.03	9.65	12.02
4017	0.52	8.42	10.17	3.42	9.27	9.45	11.66
4030	0.96	6.30	11.27	1.09	10.44	9.95	13.87
4041	0.53	11.76	10.34	0.88	9.59	9.77	11.84
4048	0.82	3.16	10.45	1.56	9.88	9.93	12.03
4216	0.86	3.97	10.69	0.52	9.78	10.50	12.39
4230	0.53	8.39	10.61	4.18	10.78	9.90	13.04
5442	0.78	10.51	10.97	2.05	10.53	10.62	13.29
6506	0.95	5.43	10.67	2.20	10.07	10.31	12.45
6749	0.77	10.04	10.87	3.34	10.76	10.04	13.33
7493	0.53	4.69	10.50	1.08	9.68	9.80	12.04
8349	0.58	4.70	10.16	2.45	9.94	9.31	11.79
8724	0.57	5.78	10.45	2.67	10.67	10.07	12.71
8914	0.54	5.32	10.32	2.91	9.75	9.92	11.85
8945	0.82	2.47	10.55	0.80	10.50	9.85	12.59
9483	0.71	3.32	10.59	0.65	10.09	9.99	12.33
9551	0.54	5.93	10.64	2.91	10.57	10.31	12.80
9704	0.53	6.83	10.73	3.38	10.55	9.48	12.90
9814	0.59	5.83	10.58	2.54	10.56	9.66	12.71

id	scale	r_{disc}	$\log M_{disc}$	$r_{1/4,bulge}$	$\log M_{bulge}$	$\log M_{gas}$	$\log M_{DMH}$
10019	0.62	8.23	10.55	1.95	10.08	10.39	12.26
10218	0.91	4.18	10.44	2.19	10.48	10.43	12.44
10841	0.54	3.62	10.18	0.48	9.89	9.52	11.78
10850	0.71	3.21	10.22	1.42	9.43	9.67	11.71
10943	0.55	3.92	10.10	1.70	9.62	9.05	11.66
10952	0.53	5.13	10.40	1.36	9.61	9.06	11.90
11019	0.72	3.57	10.05	0.93	8.05	9.24	11.53
11071	0.52	6.86	10.49	0.77	9.73	9.27	12.03
11112	0.56	6.45	10.66	3.07	10.29	10.02	12.57
11120	0.55	3.87	10.34	0.59	9.55	9.39	11.83
11223	0.71	3.81	10.57	0.72	9.78	10.03	12.18
11270	0.78	2.37	9.88	0.35	9.63	9.10	11.55
11295	0.79	10.30	10.86	3.31	10.72	10.35	13.27
11298	0.78	7.19	10.00	2.50	9.43	9.88	11.57
11311	0.68	6.25	10.72	1.46	10.47	10.22	12.82
11340	0.71	2.87	10.00	1.46	9.40	10.13	11.57
11349	0.51	4.67	10.09	2.26	9.03	9.41	11.59
11408	0.52	5.68	9.99	1.54	9.16	9.67	11.53
11845	0.72	5.01	10.58	0.93	9.38	10.12	12.11
12371	0.85	5.84	10.51	1.03	10.48	10.06	12.52
12533	0.66	5.11	9.97	2.66	9.49	9.69	11.56
13005	0.96	3.12	10.26	0.73	9.06	9.78	11.71
13074	0.95	5.02	10.62	1.81	10.48	10.40	12.66
13624	0.59	5.19	10.28	2.67	9.22	10.35	11.73
13666	0.80	2.26	10.14	0.80	9.08	9.73	11.62
14712	0.76	4.89	10.53	0.03	9.15	10.21	12.02
14831	0.87	5.89	10.94	2.10	10.87	10.17	13.57
15151	0.67	6.17	10.71	2.25	10.66	9.98	13.00
15155	0.56	8.91	10.18	8.72	8.67	10.24	11.63
15181	0.92	9.61	11.08	1.97	10.50	10.50	13.49
16655	0.67	7.51	10.39	0.82	10.26	10.14	12.16
16695	0.57	13.40	10.00	4.40	9.21	10.11	11.54
16841	0.64	4.00	9.93	2.16	9.48	10.21	11.54
17135	0.92	4.52	10.51	1.30	9.13	9.89	11.99
17865	0.54	7.96	10.25	2.00	9.13	9.83	11.71
18421	0.86	5.06	10.36	0.36	10.24	9.54	12.11
18469	0.67	3.89	10.15	0.00	0.00	9.65	11.60
18673	0.76	1.91	10.35	0.29	9.23	9.74	11.80
18686	0.81	5.02	10.48	1.55	9.73	10.46	12.02
18702	0.60	3.97	10.20	1.01	8.51	9.54	11.64
18887	0.90	4.97	10.59	1.10	10.27	9.98	12.44
19918	0.91	7.65	10.65	0.56	10.34	10.51	12.59
19949	0.58	5.66	10.59	2.37	10.01	10.13	12.28
20133	0.96	3.86	10.69	1.62	10.35	9.88	12.67

id	scale	r_{disc}	$\log M_{disc}$	$r_{1/4,bulge}$	$\log M_{bulge}$	$\log M_{gas}$	$\log M_{DMH}$
20286	0.69	5.06	10.35	1.49	10.08	9.77	12.00
22822	0.54	4.24	10.29	2.51	10.22	10.14	12.04
22999	0.89	4.46	10.62	1.33	9.42	9.95	12.19
23026	0.65	14.44	10.93	2.22	10.78	9.94	13.44
23088	0.63	9.04	10.56	2.92	9.77	9.93	12.15
23245	0.53	6.25	10.10	1.44	8.41	9.95	11.57
23320	0.54	4.06	10.02	1.74	9.42	10.06	11.58
23419	0.79	3.80	10.38	1.43	8.39	10.18	11.81
23453	0.69	4.60	10.10	1.27	8.82	9.97	11.58
23577	0.84	3.95	10.42	1.21	9.04	9.85	11.87
23685	0.92	4.26	10.36	1.06	10.44	10.41	12.31
24183	0.85	4.78	10.53	2.85	10.39	10.43	12.46
24426	0.61	5.60	10.11	1.48	8.73	10.14	11.58
24496	0.83	2.98	10.59	0.83	8.90	10.04	12.11
24973	0.57	5.80	10.59	2.68	9.31	9.93	12.13
25448	0.88	5.68	10.57	1.50	10.04	10.24	12.27
25752	0.73	5.38	10.48	1.24	9.76	10.28	12.03
25763	0.59	8.22	10.01	1.92	9.44	9.70	11.57
26040	0.61	5.38	9.94	3.01	9.12	9.92	11.50
26056	0.60	6.52	10.07	2.48	9.07	10.12	11.58
26221	0.63	10.46	10.86	1.68	10.38	10.38	12.99
26368	0.66	7.25	10.15	2.55	9.63	10.10	11.69
26570	0.65	2.99	9.95	0.92	9.08	9.21	11.50
26598	0.51	9.23	10.43	1.61	9.37	10.40	11.91
26639	0.64	4.66	10.19	1.13	9.32	9.23	11.67
26822	0.75	8.46	10.90	1.97	10.43	10.18	13.10
26958	0.83	6.73	10.76	2.15	11.09	9.85	13.68
28168	0.94	1.68	9.14	0.49	10.14	10.05	11.62
28365	0.64	7.88	10.31	2.65	9.36	10.26	11.78
29624	0.68	5.76	10.30	1.26	8.79	9.91	11.74
29842	0.68	6.79	10.63	2.59	10.30	10.01	12.53
29871	0.69	5.66	10.15	1.09	8.87	9.92	11.62
30332	0.84	6.03	10.37	3.51	9.87	9.87	11.94
30439	0.91	9.24	11.01	2.66	10.01	10.68	13.17
31188	0.87	4.72	9.98	0.96	8.85	9.65	11.50
32257	0.51	4.82	10.10	2.50	9.52	9.74	11.64
32308	0.58	5.67	9.94	2.99	9.22	9.21	11.51
32568	0.84	4.93	10.31	1.75	9.36	9.81	11.78
32619	0.96	2.07	9.88	0.69	9.40	9.65	11.50
38462	0.52	7.12	10.69	0.39	9.86	9.45	12.41
39119	0.56	4.32	10.10	1.89	9.44	9.93	11.63
39270	0.69	8.11	10.08	2.66	9.26	10.10	11.60
39548	0.69	6.78	10.34	3.35	9.65	9.84	11.84
39595	0.86	4.88	10.40	1.84	10.69	10.26	12.71

id	scale	r_{disc}	$logM_{disc}$	$r_{1/4,bulge}$	$logM_{bulge}$	$logM_{gas}$	$logM_{DMH}$
40439	0.70	11.65	10.95	4.42	8.95	10.44	12.91
40781	0.94	7.82	10.76	1.31	10.83	10.21	13.29
41728	0.56	1.18	10.18	0.00	0.00	9.73	11.62
41783	0.74	3.26	10.59	1.73	10.92	9.93	13.25
41969	0.70	3.70	10.29	2.80	9.84	10.44	11.85
42013	0.73	3.75	10.26	1.97	10.61	10.48	12.46
44710	0.71	6.89	10.07	1.21	9.44	9.72	11.61
44718	0.76	4.95	10.37	1.71	9.68	9.85	11.89
44942	0.66	6.39	10.29	2.29	9.92	9.85	11.88
47221	0.64	4.69	10.47	0.35	9.68	9.52	12.00
50550	0.70	2.87	10.22	1.53	9.43	9.73	11.71
51161	0.69	6.28	10.07	1.51	9.38	9.76	11.60
51276	0.59	6.50	10.34	3.49	9.22	10.09	11.80
51563	0.59	5.10	10.32	1.10	9.95	9.83	11.92
55541	0.85	4.97	10.61	1.09	8.92	10.17	12.14
56304	0.68	16.24	10.89	0.00	0.00	10.08	12.75
56312	0.68	4.44	9.98	1.83	9.48	10.26	11.57
56375	0.91	10.79	10.74	0.88	10.16	10.27	12.63
56632	0.56	5.78	10.73	2.71	10.67	9.72	13.03
56662	0.60	7.07	10.24	0.00	0.00	9.47	11.68
57017	0.65	5.31	10.35	1.36	10.08	9.97	12.00
101004	0.29	5.87	9.89	1.75	8.76	9.38	11.45
101007	0.35	7.05	9.44	2.17	7.75	9.56	11.20
101025	0.32	13.59	9.82	13.22	8.31	9.45	11.40
101037	0.33	6.29	9.30	1.70	7.79	9.50	11.14
108016	0.24	10.25	9.10	1.96	9.39	9.85	11.26
108021	0.35	2.27	9.60	0.58	8.59	9.19	11.30
108026	0.37	15.75	9.84	0.00	0.00	10.14	11.40
108045	0.31	8.36	9.85	7.23	9.70	10.08	11.55
108050	0.33	4.76	9.59	1.68	9.23	9.41	11.35
108051	0.29	5.52	8.88	5.12	8.72	8.47	11.05
108054	0.26	5.88	9.87	0.23	9.00	9.67	11.45
108064	0.30	7.73	9.54	1.50	8.26	9.64	11.26
108072	0.28	14.21	9.98	0.00	0.00	9.18	11.49
108093	0.34	4.43	9.90	1.93	8.84	9.33	11.46
108094	0.34	9.47	9.59	3.35	8.96	10.04	11.32
108106	0.33	1.39	9.76	0.51	9.10	9.58	11.41
108113	0.40	3.78	9.86	1.78	8.48	9.61	11.43
108142	0.39	5.58	9.61	1.90	7.61	9.57	11.28
108147	0.40	7.33	9.63	1.37	7.64	9.48	11.30
109010	0.21	11.34	9.75	0.00	0.00	9.37	11.35
109011	0.40	2.67	9.48	1.09	8.20	9.48	11.23
109028	0.36	8.59	10.06	6.30	8.37	9.96	11.54
109038	0.24	3.43	9.12	1.40	8.46	9.27	11.09

id	scale	r_{disc}	$\log M_{disc}$	$r_{1/4,bulge}$	$\log M_{bulge}$	$\log M_{gas}$	$\log M_{DMH}$
109045	0.25	8.39	9.85	9.06	8.34	8.72	11.42
109050	0.24	3.69	8.84	2.46	9.05	9.44	11.12
109058	0.33	7.16	9.87	1.84	8.81	9.69	11.44
109072	0.38	10.39	9.40	2.55	9.35	9.77	11.32
109081	0.31	7.57	9.16	6.47	8.34	9.96	11.10
109088	0.32	7.48	9.49	2.95	8.43	9.60	11.24
109092	0.36	7.42	9.70	0.00	0.00	9.38	11.33
109100	0.26	7.53	9.50	1.98	7.51	9.27	11.23
109102	0.24	8.21	9.38	0.00	0.00	9.90	11.17
109106	0.33	6.33	9.60	3.11	8.65	9.08	11.30
109108	0.21	2.56	9.53	1.53	8.87	8.88	11.29
109112	0.33	2.53	9.30	0.85	8.97	9.41	11.21
109126	0.27	3.26	9.14	0.00	0.00	8.56	11.06
109139	0.38	9.56	9.54	3.58	8.67	10.02	11.27
110013	0.36	5.53	9.69	1.99	8.41	9.29	11.33
110017	0.30	6.18	9.85	0.00	0.00	9.50	11.41
110038	0.34	5.84	9.53	1.43	9.82	9.76	11.50
110040	0.38	5.08	9.17	1.29	9.72	9.69	11.40
110041	0.35	9.55	9.93	7.18	8.23	10.14	11.46
110054	0.40	5.19	9.59	2.07	9.26	9.07	11.36
110059	0.39	9.72	9.39	2.26	8.19	9.57	11.19
110063	0.24	2.72	9.15	1.58	7.87	9.01	11.08
110080	0.30	4.61	9.19	0.95	7.20	9.37	11.09
111027	0.31	5.54	9.34	2.31	8.22	8.96	11.17
111035	0.22	16.05	9.75	0.00	0.00	9.62	11.35
111063	0.29	4.57	9.59	1.52	8.31	8.43	11.28
111067	0.40	2.41	9.27	0.00	0.00	9.56	11.12
111079	0.27	12.57	9.88	0.00	0.00	10.15	11.43
111086	0.29	5.11	9.48	4.65	9.15	8.96	11.30
111088	0.22	10.60	9.30	1.76	7.79	9.29	11.14
111091	0.35	7.10	9.67	1.14	8.48	9.89	11.33
112035	0.37	5.65	9.21	2.08	9.48	8.95	11.31
112050	0.29	2.55	8.76	1.67	9.31	9.54	11.19
112068	0.35	4.81	9.49	2.96	9.21	8.82	11.32
112090	0.21	9.36	9.67	11.57	9.69	9.88	11.49
112112	0.37	9.35	9.90	3.22	8.52	9.87	11.45
112116	0.34	2.15	9.12	0.00	0.00	9.04	11.05
113008	0.31	7.00	9.30	0.88	7.61	9.60	11.14
113062	0.34	3.30	9.86	1.13	8.91	9.51	11.44
113067	0.38	10.99	9.89	0.00	0.00	10.08	11.43
113098	0.40	4.47	9.81	1.23	8.90	9.28	11.41
113100	0.35	6.24	9.87	1.36	8.59	9.06	11.44
113118	0.33	2.94	9.12	0.00	0.00	9.07	11.05
113122	0.33	3.01	9.89	0.00	0.00	9.13	11.43

id	scale	r_{disc}	$logM_{disc}$	$r_{1/4,bulge}$	$logM_{bulge}$	$logM_{gas}$	$logM_{DMH}$
113124	0.36	8.04	9.41	0.00	0.00	9.57	11.18
113136	0.34	16.91	9.75	3.43	8.56	9.93	11.37
113141	0.28	7.20	9.54	0.00	0.00	9.20	11.25
113150	0.30	12.60	9.89	2.89	8.83	9.89	11.45
114010	0.30	6.73	9.19	0.73	9.56	8.96	11.34
114048	0.32	5.25	9.84	1.84	9.39	8.61	11.48
114113	0.35	3.27	9.07	0.00	0.00	8.96	11.03
114115	0.36	7.90	9.64	1.32	7.95	9.61	11.30
114121	0.30	8.65	9.73	2.30	8.73	9.84	11.37
114136	0.30	6.71	9.24	0.00	0.00	9.51	11.11
114141	0.30	7.03	9.45	0.00	0.00	9.86	11.20
114144	0.28	11.68	9.85	11.16	8.34	9.43	11.42
122002	0.36	7.13	9.41	3.12	8.58	9.51	11.21
122006	0.34	8.76	9.50	0.00	0.00	9.81	11.23
123006	0.31	5.65	9.83	0.69	8.32	9.58	11.41
123010	0.30	7.06	9.81	6.23	9.37	9.98	11.46
124004	0.37	4.30	9.31	0.00	0.00	9.16	11.14
124006	0.36	4.21	9.53	0.41	9.36	8.79	11.36
124010	0.36	12.36	9.93	0.00	0.00	10.40	11.46
124012	0.36	10.72	9.69	2.29	8.79	9.24	11.35

A.3 Mock-observation fit parameters

Results of finding the best-fit mock. Table includes initial values of *inc* and r_{SB}, together with best-fit parameters. Methodology described in subsection 3.3.6.

Parameter	Unit	Description
id	—	xCOLD GAS survey id, Saintonge et al. 2017
S/N	—	signal-to-noise ratio as defined in section 3.2
RMS_{obs}	mJy	RMS of observed spectrum, as defined in section 3.2
r_{SB}	arcsec	initial value of SB scaling radius, as defined in Table 3.2
inc_{kin}	°	starting value of inclination, as defined in Table 3.2
A_{fit}	—	amplitude scale of the best-fit mock line
$\mathrm{v}_{0,fit}$	$\mathrm{km\,s^{-1}}$	shift in velocity of the best-fit mock
inc_{fit}	°	best-fit inclination
r_{SBfit}	arcsec	best-fit surface brightness scaling radius

id	S/N	RMS_{obs}	r_{SB}	inc_{kin}	A_{fit}	$\mathrm{v}_{0,fit}$	inc_{fit}	$\mathrm{r}_{SB,fit}$
522	4.1	19.3	7.48	11.83	633.33	20.74	16.85	3.74
947	2.2	13.6	5.81	42.65	855.62	46.90	45.37	5.81
1115	4.9	21.0	9.30	34.71	1692.27	22.44	44.01	4.65
1137	8.8	9.1	7.52	14.97	1086.07	5.07	12.79	22.55
1221	7.6	17.9	3.62	24.16	1756.26	4.31	26.33	1.81
1977	2.5	14.2	9.04	54.16	1274.50	12.73	59.80	9.04
3261	3.7	10.6	3.03	15.16	386.19	2.96	23.56	1.51
3504	4.5	9.8	8.53	10.82	468.75	5.93	8.50	25.58
3524	1.6	5.7	2.66	41.51	322.65	0.00	41.51	5.32
3819	6.4	12.9	2.74	22.14	1934.23	31.67	20.89	5.47
3962	7.1	10.8	5.26	35.05	2344.92	16.38	41.35	5.26
3981	2.1	6.6	3.80	90.00	519.70	8.33	90.00	11.41
4017	2.2	10.7	10.38	24.68	778.54	23.01	24.68	31.14
4030	2.2	15.0	8.33	14.29	717.80	25.02	10.95	8.33
4041	2.5	10.3	9.84	52.38	690.49	23.50	64.63	9.84
4048	2.7	6.9	3.75	45.58	545.79	1.68	56.06	3.75
4216	6.1	14.1	5.03	37.59	2661.75	9.87	35.90	10.06
4230	2.2	7.4	7.77	32.61	460.85	20.70	37.02	3.89
5442	2.9	13.2	11.09	33.69	2340.56	6.18	33.69	33.28
6506	3.0	11.3	5.66	53.72	1891.29	55.23	56.12	16.97
6749	2.6	6.8	7.16	44.15	908.32	−5.13	47.23	14.32
7493	4.2	15.9	5.11	61.06	2735.53	14.42	61.06	15.32
8349	2.9	8.8	4.16	69.88	736.53	9.50	90.00	4.16
8724	2.2	16.0	5.35	55.31	1709.68	11.00	55.31	16.05
8914	2.5	16.0	6.98	47.02	1516.85	16.87	44.35	20.93
8945	2.0	9.8	2.70	53.02	757.23	14.36	53.02	1.35
9483	3.8	12.1	4.44	24.43	1048.97	−0.48	22.93	13.31

id	S/N	RMS_{obs}	r_{SB}	inc_{kin}	A_{fit}	$v_{0,fit}$	inc_{fit}	$r_{SB,fit}$
9551	5.5	18.6	5.49	63.33	5992.26	25.60	60.73	16.48
9704	2.2	9.4	6.33	90.00	1261.05	13.46	90.00	18.98
9814	3.1	16.5	7.19	24.08	994.92	5.59	26.98	3.60
10019	2.8	13.6	7.18	50.20	1456.64	2.89	55.36	14.37
10218	2.8	14.2	5.00	30.03	1133.32	42.45	36.61	2.50
10841	2.3	5.6	3.39	56.67	400.42	18.63	56.67	1.70
10850	1.7	7.8	3.41	58.89	371.43	9.36	67.99	6.81
10943	1.5	11.1	4.12	48.39	321.62	−15.19	39.28	2.06
10952	1.6	9.8	4.44	75.47	627.16	27.25	90.00	13.32
11019	2.2	10.9	3.76	40.40	435.43	19.96	54.86	3.76
11071	1.7	9.9	7.09	35.89	464.81	18.23	33.77	14.18
11112	6.5	13.1	5.97	57.96	4386.61	20.53	55.48	17.92
11120	1.8	12.1	3.87	66.84	769.60	14.62	62.55	11.61
11223	10.2	7.3	4.45	67.78	2762.75	2.23	72.21	4.45
11270	1.6	7.8	2.41	32.35	167.75	8.33	29.59	1.21
11295	1.9	8.1	6.41	73.38	1058.67	4.40	90.00	19.24
11298	1.8	7.4	4.55	65.27	373.70	5.23	71.80	13.66
11311	2.7	10.6	4.88	56.98	1421.67	−3.09	59.30	14.64
11340	4.0	8.9	3.47	70.06	1005.41	−4.27	90.00	3.47
11349	3.0	13.9	5.54	51.46	847.71	−4.78	41.41	5.54
11408	5.7	14.6	6.93	11.36	672.00	19.98	13.82	3.46
11845	3.5	14.3	5.31	51.13	1521.57	−6.90	59.59	5.31
12371	1.6	11.3	4.69	32.74	581.72	4.98	36.08	14.07
12533	7.6	13.7	6.51	16.79	827.07	1.71	19.28	3.26
13005	3.4	12.3	4.42	37.33	1206.46	56.47	39.97	4.42
13074	2.1	12.9	4.12	52.11	1336.77	54.18	56.44	12.36
13624	3.3	16.1	6.44	48.78	1520.55	6.66	48.78	12.89
13666	3.9	10.1	3.31	75.05	1125.13	11.00	75.05	3.31
14712	7.7	16.6	6.76	19.18	1918.63	2.16	22.33	6.76
14831	1.8	12.5	5.00	39.24	827.05	−25.37	39.24	2.50
15151	3.8	7.2	4.61	71.27	1518.59	1.48	75.31	13.84
15155	5.2	12.6	8.25	90.00	2416.52	72.84	90.00	16.50
15181	2.3	7.3	7.36	38.64	1198.90	44.00	39.90	22.09
16655	2.1	7.7	4.54	90.00	679.31	6.28	90.00	13.61
16695	1.6	10.1	7.06	90.00	549.68	6.85	90.00	21.19
16841	3.3	11.1	5.42	27.51	606.55	2.09	25.10	10.85
17135	1.9	11.1	4.19	52.39	714.34	26.74	55.35	8.38
17865	2.6	12.1	9.00	39.57	830.73	16.63	34.16	18.00
18421	2.0	10.9	3.63	21.97	420.93	17.26	26.19	3.63
18469	2.2	9.5	5.31	46.97	552.71	3.01	43.78	15.94
18673	2.9	13.4	2.67	45.15	1128.04	5.07	47.55	8.01
18686	2.4	9.4	5.74	67.62	876.83	11.00	63.68	11.48
18702	2.2	8.0	3.85	90.00	544.83	3.46	74.20	7.71
18887	1.8	5.6	3.66	76.34	483.57	40.75	90.00	10.97

id	S/N	RMS_{obs}	r_{SB}	inc_{kin}	A_{fit}	$v_{0,fit}$	inc_{fit}	$r_{SB,fit}$
19918	1.7	7.0	5.70	52.22	550.59	33.00	59.32	11.41
19949	3.7	14.5	6.83	37.70	1489.02	9.71	43.58	6.83
20133	1.8	11.2	4.81	30.34	903.48	55.00	30.34	14.43
20286	1.8	13.3	3.88	90.00	960.50	3.59	90.00	11.64
22822	2.9	16.0	4.21	58.99	1750.75	15.79	55.98	12.64
22999	2.9	15.8	4.65	32.36	1059.12	21.31	40.15	4.65
23026	2.3	10.7	7.48	90.00	1719.46	−4.52	90.00	22.45
23088	3.2	11.7	9.08	53.49	1499.97	−7.36	67.43	18.17
23245	2.7	17.3	8.56	5.07	481.93	12.22	0.00	17.13
23320	2.3	10.0	5.60	52.67	734.06	13.83	49.27	16.81
23419	2.6	11.8	4.20	53.12	976.73	13.59	50.17	12.61
23453	1.7	9.6	6.37	90.00	549.74	5.30	90.00	12.74
23577	3.3	16.8	4.90	37.24	1166.30	14.05	39.61	4.90
23685	2.5	11.4	3.33	69.66	1064.88	3.21	56.78	6.67
24183	4.1	13.8	5.94	39.60	2402.10	17.94	39.60	17.81
24426	3.2	9.4	7.23	44.42	965.88	12.82	41.43	21.68
24496	3.6	8.5	3.61	54.08	1097.90	9.05	66.44	3.61
24973	29.1	16.4	5.37	10.41	4005.78	9.63	15.33	2.68
25448	1.8	9.8	6.84	20.94	387.05	27.69	20.94	13.69
25752	5.3	13.0	7.11	16.48	1188.36	3.82	14.76	21.33
25763	5.8	15.9	8.07	16.32	804.82	4.59	21.46	4.04
26040	2.0	7.2	5.71	47.22	354.88	2.29	47.22	17.12
26056	2.2	9.9	7.73	65.80	771.98	17.96	65.80	23.18
26221	11.9	7.4	7.81	59.31	5571.78	0.68	61.80	23.43
26368	2.4	11.5	5.51	90.00	962.73	8.29	90.00	16.53
26570	3.4	5.5	4.22	57.87	439.57	4.34	53.46	12.67
26598	2.7	12.6	10.13	47.80	982.00	23.44	56.94	10.13
26639	1.7	9.2	4.32	56.92	398.31	−5.28	49.62	12.97
26822	3.7	11.9	7.10	46.27	2554.08	−2.93	46.27	21.31
26958	4.7	9.0	6.23	62.14	2848.50	12.84	64.16	12.46
28168	1.7	7.2	1.37	28.84	285.77	34.93	30.81	0.69
28365	7.8	16.3	10.40	22.49	2419.42	4.28	20.34	20.80
29624	2.4	13.9	5.11	75.35	1140.25	6.65	90.00	15.33
29842	2.3	15.2	5.97	90.00	1828.17	−8.25	90.00	17.91
29871	2.4	7.1	6.28	73.02	425.33	9.62	66.59	6.28
30332	4.6	12.8	6.68	53.24	1977.24	10.28	59.93	13.37
30439	4.1	13.9	8.69	48.76	4171.43	41.04	50.43	26.08
31188	2.2	9.3	5.85	9.39	246.37	20.84	6.90	5.85
32257	5.0	14.5	5.99	41.72	1475.44	23.98	54.81	3.00
32308	2.9	9.7	8.09	17.66	324.85	5.14	17.66	16.18
32568	4.7	6.6	5.58	90.00	1058.23	14.51	90.00	11.16
32619	3.0	5.0	2.74	53.99	383.32	53.07	77.82	1.37
38462	2.7	16.2	6.83	49.35	1823.74	24.21	51.65	13.67
39119	2.9	13.5	4.18	33.29	778.01	29.92	41.34	4.18

id	S/N	RMS_{obs}	r_{SB}	inc_{kin}	A_{fit}	$v_{0,fit}$	inc_{fit}	$r_{SB,fit}$
39270	2.4	10.0	9.71	38.27	574.17	0.00	38.27	19.42
39548	2.6	11.8	7.73	47.87	1111.12	4.41	50.88	23.18
39595	2.6	10.1	4.25	60.94	1346.92	12.74	70.18	12.76
40439	4.8	14.5	10.79	26.22	3039.82	1.84	26.22	32.36
40781	2.0	10.2	4.31	48.89	1206.85	53.42	53.84	12.94
41728	2.0	9.9	1.09	44.20	582.05	11.00	42.20	2.18
41783	1.9	8.1	3.29	71.75	917.16	15.22	80.16	1.64
41969	5.4	17.8	5.98	17.89	1174.88	0.54	17.89	5.98
42013	6.4	14.8	3.96	41.60	2796.14	−3.27	43.42	1.98
44710	2.4	7.6	6.00	42.43	276.18	−37.16	30.84	3.00
44718	6.5	10.5	5.45	49.52	2232.25	6.97	49.52	16.36
44942	3.0	17.8	6.27	90.00	2095.31	0.09	90.00	18.81
47221	1.8	11.2	5.05	46.47	589.69	1.04	46.47	10.10
50550	2.2	16.8	3.73	65.31	1095.83	2.61	70.57	3.73
51161	2.5	14.0	5.63	55.23	1010.98	5.27	59.52	16.89
51276	3.5	11.1	6.04	55.92	1064.69	8.73	74.58	6.04
51563	2.1	14.2	5.02	50.82	812.86	1.01	50.82	5.02
55541	3.0	12.3	5.04	60.90	1441.63	18.55	73.07	10.08
56304	1.6	10.0	15.04	42.58	1120.76	−11.00	38.67	45.11
56312	2.0	10.0	4.59	64.68	519.44	9.49	90.00	4.59
56375	2.5	14.6	9.41	10.68	519.54	38.69	13.49	4.70
56632	4.3	6.5	5.35	90.00	1708.95	12.45	78.51	16.05
56662	2.9	8.6	6.67	90.00	875.05	−14.72	90.00	20.00
57017	2.1	6.3	3.93	64.22	488.58	−13.01	90.00	11.80
101004	4.3	12.4	5.85	61.46	1190.08	5.33	90.00	5.85
101007	2.4	10.0	8.63	26.03	348.59	0.00	26.03	25.88
101025	4.4	28.9	12.58	15.27	878.39	2.02	21.91	6.29
101037	1.7	9.6	6.40	39.27	292.20	−5.18	35.00	19.19
108016	4.2	21.6	8.11	15.66	547.60	3.44	15.66	4.05
108021	3.7	17.1	3.36	42.98	1140.41	1.02	39.34	10.08
108026	6.6	20.8	14.58	18.83	1137.56	1.30	22.10	7.29
108045	10.4	17.3	7.74	38.05	3203.11	2.72	44.32	7.74
108050	2.8	18.6	5.25	50.37	858.75	2.66	66.53	2.63
108051	2.1	11.1	5.11	12.69	83.27	−0.57	12.69	5.11
108054	2.9	24.5	6.29	34.89	1646.73	−2.09	34.89	18.86
108064	2.8	10.8	7.54	36.05	449.70	−6.04	53.77	7.54
108072	3.0	22.1	13.16	48.46	1079.35	−8.03	73.28	6.58
108093	3.6	18.6	4.96	57.00	1400.02	−0.37	61.91	4.96
108094	8.4	25.4	9.12	10.76	948.71	−1.35	13.75	4.56
108106	6.6	30.6	2.15	31.63	3600.72	3.15	31.63	1.08
108113	2.7	10.5	5.34	57.22	728.56	2.95	52.85	16.01
108142	1.7	8.4	6.66	52.15	344.70	−7.49	52.15	19.98
108147	1.9	11.7	9.46	34.22	508.59	−7.28	34.22	28.37
109010	2.8	25.7	10.50	90.00	2003.78	1.03	90.00	31.51

id	S/N	RMS_{obs}	r_{SB}	inc_{kin}	A_{fit}	$v_{0,fit}$	inc_{fit}	$r_{SB,fit}$
109011	1.5	9.6	4.27	33.21	197.84	3.63	33.21	8.53
109028	3.3	22.4	7.95	79.49	2184.60	−3.53	90.00	15.91
109038	1.9	13.4	3.76	52.74	448.82	10.29	66.58	7.53
109045	3.2	12.7	7.77	69.47	1011.76	0.00	90.00	15.54
109050	2.5	9.8	5.15	20.77	259.58	0.00	20.77	15.45
109058	2.0	18.5	6.70	56.10	788.32	−4.77	75.07	6.70
109072	2.0	11.2	5.77	90.00	549.71	−5.19	63.14	17.30
109081	2.6	15.6	7.01	33.18	627.83	5.39	25.71	21.02
109088	1.5	13.2	8.89	52.15	504.45	0.29	52.15	26.68
109092	1.8	13.2	6.64	48.78	523.47	−2.01	48.78	19.91
109100	1.6	12.2	7.87	90.00	494.38	0.00	90.00	23.62
109102	1.5	9.0	8.02	90.00	349.46	−12.35	90.00	16.04
109106	3.4	14.6	7.73	41.81	719.59	7.17	61.92	3.87
109108	2.9	30.1	3.34	46.21	1703.95	14.31	58.95	3.34
109112	2.4	12.2	2.95	43.07	378.32	−17.13	35.23	1.48
109126	4.0	13.0	4.40	17.88	295.92	−3.03	22.01	2.20
109139	1.7	14.9	10.13	61.03	613.83	−7.70	78.83	20.25
110013	1.7	25.2	6.39	49.08	989.96	6.21	49.08	19.16
110017	3.7	22.0	5.73	37.63	1648.95	−1.97	37.63	17.18
110038	2.4	15.8	3.87	49.66	785.26	2.64	46.03	7.75
110040	2.9	17.5	3.99	11.51	334.73	1.14	6.09	11.96
110041	4.4	23.6	8.84	39.98	1957.69	0.46	55.34	8.84
110054	2.6	10.4	5.22	24.20	357.74	−7.75	30.77	10.44
110059	1.7	4.9	10.31	44.93	98.27	−6.78	50.02	5.15
110063	2.3	9.4	4.43	32.85	291.39	0.00	28.57	13.28
110080	2.8	9.5	4.85	80.44	549.60	−3.39	90.00	14.54
111027	2.3	11.7	6.32	54.27	450.48	5.83	54.27	12.64
111035	3.1	19.3	14.86	51.63	1048.89	−11.95	57.60	14.86
111063	2.9	12.3	5.47	49.35	655.75	0.00	44.74	16.41
111067	2.2	5.7	3.10	27.00	140.32	−42.67	30.60	1.55
111079	3.3	17.7	11.64	32.43	756.90	−1.55	47.22	5.82
111086	2.3	11.8	4.73	60.22	523.01	5.29	67.28	9.47
111088	2.0	13.0	8.48	41.57	537.50	5.89	68.94	25.44
111091	2.6	16.0	10.74	17.68	265.34	16.18	6.25	5.37
112035	6.9	15.9	6.03	25.25	920.65	−1.64	21.86	6.03
112050	2.9	13.6	3.25	27.64	436.88	−2.91	24.28	9.75
112068	1.7	20.8	7.47	47.52	791.44	0.00	43.16	22.41
112090	13.4	21.1	8.66	90.00	9566.99	9.10	90.00	25.99
112112	2.3	23.1	7.93	65.39	1599.04	−14.14	65.39	23.79
112116	3.5	12.0	3.24	58.07	591.78	−12.49	36.13	9.71
113008	2.0	11.3	8.71	60.47	575.14	8.98	60.47	26.12
113062	3.9	22.6	3.76	90.00	2521.22	1.21	90.00	7.52
113067	2.7	19.2	10.18	38.96	1366.81	−1.64	38.96	30.53
113098	2.2	14.8	3.99	90.00	859.12	10.96	90.00	11.96

id	S/N	RMS_{obs}	r_{SB}	inc_{kin}	A_{fit}	$v_{0,fit}$	inc_{fit}	$r_{SB,fit}$
113100	3.6	19.8	6.00	90.00	1937.44	2.08	90.00	18.00
113118	1.9	7.1	4.54	18.93	103.89	6.33	15.07	13.62
113122	2.1	30.9	3.72	51.71	1607.76	5.11	55.71	11.16
113124	1.6	8.7	8.08	53.98	347.91	29.96	90.00	24.25
113136	2.4	13.3	11.40	48.73	459.75	17.36	53.92	5.70
113141	2.2	18.6	8.63	42.32	909.18	1.88	42.32	25.90
113150	2.5	17.9	10.09	64.97	1156.70	4.95	90.00	20.18
114010	1.7	11.8	2.19	66.81	456.08	1.64	66.81	4.37
114048	1.8	10.7	6.69	13.77	148.50	−6.67	16.43	6.69
114113	2.0	6.8	4.60	15.24	55.44	−3.22	11.33	4.60
114115	2.6	11.0	7.45	53.22	593.27	5.42	58.65	14.90
114121	2.7	14.4	8.13	79.79	967.74	2.03	79.79	16.25
114136	2.2	12.6	9.63	23.21	419.12	0.50	23.21	28.88
114141	1.6	12.9	9.27	32.71	244.00	−17.61	48.89	4.64
114144	7.7	18.7	10.81	60.58	4145.44	1.67	90.00	32.43
122002	2.0	8.6	6.38	60.18	351.07	−20.56	44.13	19.15
122006	2.6	7.7	8.11	35.01	409.20	1.35	35.01	24.34
123006	5.3	15.0	7.80	32.57	1036.75	−0.99	42.45	3.90
123010	15.2	19.0	6.53	24.96	3267.25	6.61	27.69	6.53
124004	1.9	15.7	6.11	21.00	231.49	−2.41	36.79	3.06
124006	2.7	11.7	3.35	42.02	497.92	−1.94	42.02	1.67
124010	5.3	23.0	11.45	28.35	2321.76	−2.18	25.38	22.89
124012	2.1	13.4	6.70	64.97	579.31	−4.27	90.00	13.39

B Galaxy modeling class

Python class used to generate mock cubes, extract spectra and fit mocks

```
class gal_model:

    # initialization of class
    def __init__(self, params, inc_var = True):

        # index parameter for distinguishing between different model parameters
        self.ind = 0 # default, change during iteration through diff. combinations

        # saving params as inner value
        self.params = params

        # galaxy information
        self.id = params['id'].values
        self.M_star = params['logMstar'].values
        self.z = params['z'].values
        self.scale = params['scale'].values
        self.W50_CO = params['W50_CO'].values
        self.Vmax = params['Vmax'].values

        # SB profile params
        self.r_SB = params['r_SB'].values

        # velocity profile params
        self.M_disc = params['M_disc'].values
        self.r_disc = params['r_disc'].values
        self.M_gas = params['M_gas'].values
        self.M_HI = params['M_HI'].values
        self.M_H2 = params['M_H2'].values

        self.BT_g = params['B/T_g'].values
        self.BT_r = params['B/T_r'].values
        self.M_bulge = params['M_bulge'].values
        self.r14_bulge = params['r14_bulge'].values

        self.M_DMH = params['M_DMH'].values

        self.inc = params['inc'].values
        self.inc_kin = params['inc_kin'].values
        self.pos_angle = 0 # not relevant, axial symmetry
        self.gas_sigma = 10 # assuming constant dispersion


        # model cube parameters
        ## axis params
        self.xsize = 105
        self.ysize = 105
        self.vsize = 881
        self.dx = 1
        self.dv = 11
```

```
50
51          ## cube center
52          self.cent = [(self.xsize / 2), (self.ysize / 2), (self.vsize /
                        2)]
53
54          ## beam size
55          self.beam = [22, 22, 0]
56
57          ## CO(1-0) rest frequency
58          self.rest_freq = 115.271202e9 # Hz
59
60          # files paths
61
62          ## filename
63          self.filename = params['filename'].values
64
65          ## mock folder
66          self.mocks_dir = f'./Data/Processed/Mocks/Corr/CO/G{self.id[0]}
                        '
67
68          ## observed spectrum
69          self.obs_path = f'./Data/Processed/Shift&regrid/CO10/G{self.id
                        [0]}_CO10.txt'
70
71          ### reading observed spectrum
72          self.obs_spec = pd.read_csv(self.obs_path, sep = '\s+', comment
                         = '#')
73
74          # modeling profiles
75          self.model_profiles = pd.read_csv(f'{self.mocks_dir}/G{self.id
                        [0]}_model_profiles.txt', sep = '\s+',
                        comment = '#')
76          self.rad_prof = self.model_profiles['rad_prof'].values
77          self.vel_prof = self.model_profiles['vel_prof'].values
78          self.sb_prof = [self.gen_sb_prof(ind = a) for a in range(len(
                        self.inc))]
79
80
81          # mock spectra list
82          self.cube_path = ['' for i in range(len(self.inc))]
83          self.mock_spec = [0 for i in range(len(self.inc))]
84          self.fit_A = [0 for i in range(len(self.inc))]
85          self.fit_x0 = [0 for i in range(len(self.inc))]
86          self.fit_chi2 = [0 for i in range(len(self.inc))]
87          self.mock_fit_spec = [0 for i in range(len(self.inc))]
88
89          ### retrieving observation parameters
90          # RMS
91          self.RMS_obs = params['RMS'].values
92          self.AN_obs = params['AN'].values
93          self.SN_obs = params['SN'].values
94
95
96
97
```

```
98      # galaxy modeling method
99      # @jit(forceobj = True)
100     def model_disc(self, kin_inc = False):
101
102         i = self.ind
103
104         # initializing KinMS
105         kinms = KinMS(self.xsize, self.ysize, self.vsize, self.dx, self
                                .dv, \
106                       nSamps = 1e6, beamSize = self.beam, verbose =
                                                  False)
107
108         #modelling galaxy cube
109         cube = kinms.model_cube(sbRad = self.rad_prof, sbProf = self.
                                sb_prof[i], velProf = self.vel_prof, \
110                                 inc = self.inc[i], posAng = self.
                                                      pos_angle,
                                                      restFreq = self
                                                      .rest_freq, \
111                                 gasSigma = self.gas_sigma, toplot =
                                                      False)
112
113         # getting beam unit from kinms for fits header
114         self.bunit = kinms.bunit
115
116         # saving to fits
117         #self.save_to_fits(cube)
118
119
120
121         # hdu initialization and header parameters input
122         hdu = fits.PrimaryHDU(cube.T)
123         hdu.header['CDELT1'] = (self.dx / -3600)
124         hdu.header['CDELT2'] = (self.dx / 3600)
125         hdu.header['CDELT3'] = self.dv
126         hdu.header['CRPIX1'] = (self.cent[0] + 1)
127         hdu.header['CRPIX2'] = (self.cent[1] + 1)
128         hdu.header['CRPIX3'] = 1
129         hdu.header['CRVAL1'] = 0.0
130         hdu.header['CRVAL2'] = 0.0
131         hdu.header['CRVAL3'] = -self.cent[2] + 0.5, 'km/s'
132         hdu.header['CUNIT1'] = 'deg'
133         hdu.header['CUNIT2'] = 'deg'
134         hdu.header['CUNIT3'] = 'km/s'
135         hdu.header['BSCALE'] = 1.0
136         hdu.header['BZERO'] = 0.0
137         hdu.header['BMIN'] = (self.beam[1] / 3600)
138         hdu.header['BMAJ'] = (self.beam[0] / 3600)
139         hdu.header['BTYPE'] = 'Intensity'
140         hdu.header['BPA'] = (self.beam[2])
141         hdu.header['CTYPE1'] = 'RA---SIN'
142         hdu.header['CTYPE2'] = 'DEC--SIN'
143         hdu.header['CTYPE3'] = 'VRAD'
144         hdu.header['EQUINOX'] = 2000.
145         hdu.header['RADESYS'] = 'FK5'
```

```
146         hdu.header['BUNIT'] = self.bunit
147         hdu.header['SPECSYS'] = 'BARYCENT'
148         hdu.header['RESTFRQ'] = self.rest_freq
149 
150         # Saving into .fits file
151         self.cube_path[i] = f'{self.mocks_dir}/{self.filename[i]}_cube.
                                fits'
152         hdu.writeto(self.cube_path[i], overwrite=True, output_verify='
                                fix')
153 
154         return # cube
155 
156 
157     # extracting spectrum
158     def get_spectrum(self, radius):
159 
160         # identification of model to use
161         i = self.ind
162 
163         # opening the data-cube
164         cube = SpectralCube.read(self.cube_path[i])
165 
166         # extracting parameters from header
167         # hdu = fits.open(self.cube_path[i])[0]
168         dx = (self.dx / 3600) # hdu.header['CDELT2'] # degree
169         x_cent = (self.cent[0] + 1) # hdu.header['CRPIX1'] - 1 # px
170         y_cent = (self.cent[1] + 1) # hdu.header['CRPIX2'] - 1 # px
171 
172         # creating circular aperture
173         yy, xx = np.indices([radius * 2 + 1, radius * 2 + 1], dtype='
                                float')
174         rad = ((yy-radius)**2 + (xx-radius)**2)**0.5
175         mask = rad <= radius + 0.5
176 
177         # applying aperture and retrieving spectra
178         shape = np.shape(cube)
179         subcube = cube[:, int(x_cent - int(radius)) : int(x_cent + int(
                                radius) + 1), int(y_cent - int(radius))
                                 : int(y_cent + int(radius) + 1)]
180         maskedsubcube = subcube.with_mask(mask)
181         spectrum = maskedsubcube.sum(axis=(1,2))
182 
183         # saving spectrum to file
184         data = np.array([cube.spectral_axis.value ,spectrum.value]).T
185         spectrum_DF = pd.DataFrame(data , columns = ['vel', 'flux'])
186         self.mock_spec[i] = spectrum_DF
187         comment = f'# Modelled spectrum for galaxy G{self.id[i]}
                                extracted from data-cube created using
                                KinMS package,' \
188                   '# spectral_cube package used for manipulation and
                                        extraction. \n'
189 
190 
191         to_unified_format( f'{self.mocks_dir}/{self.filename[i]}.txt',
                                spectrum_DF, comment)
```

```
192
193         # plotting the spectra
194         plt.figure(figsize = [12.8, 9.6])
195         plt.plot(spectrum_DF['vel'], spectrum_DF['flux'], color = 'b')
196         plt.axvline(0)
197         plt.xlabel('velocity [km/s]', fontsize = 14)
198         plt.ylabel('flux [mJy]', fontsize = 14)
199         plt.title(f'G{self.filename[i]}_model', fontsize = 20)
200
201         plt.savefig(f'{self.mocks_dir}/{self.filename[i]}.png', dpi =
                                300)
202
203         plt.close()
204
205         return # spectrum_DF
206
207
208
209     # ploting profiles
210     def plot_profiles(self):
211
212         # identification of model to use
213         i = self.ind
214
215         # extracting profiles for ploting
216
217         # maximal ploted radii
218         r_max_kpc = 30
219         r_max = r_max_kpc / self.scale[i]
220         R_max = 0
221         for a in self.rad_prof:
222             if a <= r_max:
223                 R_max += 1
224             else:
225                 break
226         R_max = int(R_max)
227
228         rad_prof = self.rad_prof[0:R_max] * self.scale[i]
229         sb_prof = self.sb_prof[i][0:R_max]
230         vel_prof = self.vel_prof[0:R_max]
231         v_s_prof = self.model_profiles['v_stellar'][0:R_max]
232         v_g_prof = self.model_profiles['v_gas'][0:R_max]
233         v_bulge_prof = self.model_profiles['v_bulge'][0:R_max]
234         v_DMH_prof = self.model_profiles['v_DMH'][0:R_max]
235
236         # initializing fig ax objects
237         fig, ax = plt.subplots(figsize = [12.8, 9.6])
238
239         # plotting SB profile
240         ax.plot(rad_prof, sb_prof, label = 'SB', color = 'g')
241         ax.axvline(self.r_SB[i] * self.scale[i], label = 'r_SB', color
                                = 'g', linestyle = '--')
242
243         # init. second y axis
244         ax_twin = ax.twinx()
```

```
245
246             # plotting velocity profile
247             ax_twin.plot(rad_prof, vel_prof, label = 'cicular velocity',
                                color = 'b')
248             ax_twin.plot(rad_prof, v_s_prof, label = 'stellar', color = '
                                grey', linestyle = ':')
249             ax_twin.plot(rad_prof, v_g_prof, label = 'gas', color = 'grey',
                                 linestyle = '--')
250             ax_twin.plot(rad_prof, v_bulge_prof, label = 'bulge', color = '
                                grey', linestyle = '-.')
251             ax_twin.plot(rad_prof, v_DMH_prof, label = 'DM halo', color = '
                                grey', linestyle = (0, (3, 5, 1, 5, 1,
                                5)))
252             # ax_twin.axvline(self.r_disc[i] * self.scale[i], label = '
                                r_disc', color = 'b', linestyle = ':' )
253
254             # styling the plot
255             ax.set_xlabel('radius [kpc]', fontsize = 14)
256             ax.set_ylabel('SB', color = 'g', fontsize = 14)
257             ax_twin.set_ylabel('velocity [km/s]', color = 'b', fontsize =
                                14)
258             ax_twin.legend(loc = 'right', fontsize = 12)
259             ax.legend(loc = 'lower right', fontsize = 12)
260             ax.set_title(f'{self.filename[i]} profiles', fontsize = 20)
261             ax.minorticks_on()
262             ax_twin.minorticks_on()
263
264             # saving profiles plot
265             fig.savefig(f'{self.mocks_dir}/{self.filename[i]}_profiles.png'
                                ) #f'{self.mocks_dir}/G{self.id}/G{self
                                .id}_model_profiles.png', dpi = 600)
266
267             # closing figure
268             plt.close()
269
270             return
271
272
273
274         # comprison with observation
275         def obs_comp_plot(self, mock = True, fit = False):
276
277             # identification of model to use
278             i = self.ind
279
280             # maximum ploted velocity
281             v_plot = 429
282
283             obs_spec = self.obs_spec
284
285             # observation peak value
286             obs_peak = max(self.obs_spec['flux'])
287
288             # extracting subsets
289             obs_vel = self.obs_spec[self.obs_spec['vel'].between(-v_plot,
```

```
                                v_plot)]['vel'].values
290         obs_flux = self.obs_spec[self.obs_spec['vel'].between(-v_plot,
                                v_plot)]['flux'].values
291
292
293         # ploting spectra
294
295         ## initializing figure
296         fig, (ax1, ax2) = plt.subplots(2, 1, figsize=(12.4, 9.8),
                                gridspec_kw={'height_ratios': [5, 1]})
297
298         ## Upper plot - mock x obs
299         ax1.plot(obs_vel, obs_flux, label = 'obs', color = 'blue')
300         ax1.fill_between(obs_vel, obs_flux - self.RMS_obs[i], obs_flux
                                + self.RMS_obs[i], alpha = 0.5, \
301                         color = 'lightblue', label = 'RMS error')
302         ax1.hlines(y = [self.RMS_obs[i], -self.RMS_obs[i]], xmin = min(
                                obs_vel), xmax = max(obs_vel),
303                    linestyles = 'dashed', label = 'obs. RMS')
304         ax1.axvline(0, linewidth = 0.5, color = 'grey')
305         ax1.axhline(0, linewidth = 0.5, color = 'grey')
306
307         ### upper plot visuals
308         ax1.minorticks_on()
309         ax1.set_xlabel('velocity [km/s]', fontsize = 14)
310         ax1.set_ylabel('flux [mJy]', fontsize = 14)
311         ax1.set_title(f'ID: {self.filename[i]}', fontsize = 20)
312
313
314         ## Lower plot - residuals
315         ax2.hlines(y = [1, -1], xmin = min(obs_vel), xmax = max(obs_vel
                                ),
316                    linestyles = 'dashed', label = 'obs RMS')
317         ax2.hlines(y = [3, -3], xmin = min(obs_vel), xmax = max(obs_vel
                                ),
318                    linestyles = 'dotted', label = r'3sigma limit')
319         ax2.axhline(0, linewidth = 0.5, color = 'grey')
320         ax2.axvline(0, linewidth = 0.5, color = 'grey')
321
322         ### lower plot visuals
323         ax2.minorticks_on()
324         ax2.set_xlabel('velocity [km/s]', fontsize = 14)
325         ax2.set_ylabel('relative flux', fontsize = 14)
326         ax2.set_title('residuals', fontsize = 14)
327
328         if mock:
329             mock_spec = self.mock_spec[i]
330
331             mock_peak = max(self.mock_spec[i]['flux'])
332
333             mock_spec['flux_scaled'] = obs_peak / mock_peak * self.
                                mock_spec[i]['flux']
334
335             mock_vel = mock_spec[mock_spec['vel'].between(-v_plot,
                                v_plot)]['vel'].values
```

```
336             mock_flux_scaled = mock_spec[mock_spec['vel'].between(-
                                    v_plot, v_plot)]['flux_scaled'].
                                    values
337
338             ax1.plot(mock_vel, mock_flux_scaled, label = 'mock', color
                                    = 'red')
339             ax2.plot(obs_vel, (obs_flux - mock_flux_scaled)/self.
                                    RMS_obs[i], label = '(obs - mock)/
                                    RMS', color = 'red')
340
341         if fit:
342             fit_spec = self.mock_fit_spec[i]
343             fit_vel = fit_spec[fit_spec['vel'].between(-v_plot, v_plot)
                                    ]['vel'].values
344             fit_flux = fit_spec[fit_spec['vel'].between(-v_plot, v_plot
                                    )]['flux'].values
345
346             # fit param extraction
347             x0 = round(self.fit_x0[i], 1)
348             A = round(self.fit_A[i])
349             chi2 = round(self.fit_chi2[i], 2)
350
351             # plotting fit of the mock
352             ax1.plot(fit_vel, fit_flux, label = f'mock fit: \n A = {A}
                                    \n v0 = {x0} \n chi2 = {chi2}',
                                    color = 'green')
353
354             # plotting fit residuals
355             ax2.plot(obs_vel, (obs_flux - fit_flux)/self.RMS_obs[i],
                                    label = '(obs - mock_fit)/RMS',
                                    color = 'green')
356
357         # plotting legends
358         ax1.legend(fontsize = 12, loc = 'upper right')
359         ax2.legend(fontsize = 12, loc = 'right')
360
361         fig.tight_layout(pad = 1.3)
362         # Svaing figure
363         fig.savefig(f'{self.mocks_dir}/{self.filename[i]}_obs_comp.png'
                                , dpi = 300)
364
365         # closing figure
366         plt.close()
367
368         return
369
370
371
372     # mock fitting method
373     def fit_mock(self, no_shift = False):
374
375         # identification of model to use
376         i = self.ind
377
378         # retrieving spectra DataFrames
```

```
379         obs_spec = self.obs_spec
380         mock_spec = self.mock_spec[i]
381
382         # limitting velocity range
383         vlim = 429
384
385         obs_spec = obs_spec[obs_spec['vel'].between(-vlim, vlim)]
386         mock_spec = mock_spec[mock_spec['vel'].between(-(vlim), vlim)]
387
388         obs_line = obs_spec[obs_spec['vel'].between(-self.W50_CO[i]/2,
                                self.W50_CO[i]/2)]['flux']
389         mock_line = mock_spec[mock_spec['vel'].between(-self.W50_CO[i
                                ]/2, self.W50_CO[i]/2)]['flux']
390
391         peak_ratio = obs_line.max() / mock_line.max() # used for bounds
                                 on amplitude of fit
392
393         # extracting values for fitting
394         xdata = obs_spec['vel'].values
395         ydata = obs_spec['flux'].values
396
397         xmock = mock_spec['vel'].values
398         ymock = mock_spec['flux'].values
399
400         # fit bounds
401         bounds = ([0.5*peak_ratio, -self.W50_CO[i]/2], [1.5*peak_ratio,
                                self.W50_CO[i]/2])
402
403         if no_shift:
404             bounds([0.5*peak_ratio,0], [1.5*peak_ratio,0])
405
406         # sigma value list
407         sigma = [self.RMS_obs[i] for a in range(len(xdata))]
408
409         # fitting 'function'
410         popt, pcov = curve_fit(self.mock_fun, xdata, ydata, sigma =
                                sigma, bounds = bounds)
411         fit_error = np.sqrt(np.diag(pcov))
412
413         fit_mock_spec = pd.DataFrame(np.array([self.mock_spec[i]['vel'
                                ], self.mock_fun(self.mock_spec[i]['vel
                                '], popt[0], popt[1])]).T, columns = ['
                                vel', 'flux'])
414         yfit = fit_mock_spec[fit_mock_spec['vel'].between(-vlim, vlim)
                                ]['flux']
415         # calculating goodness of fit
416
417         ## using RMS of residuals
418         resid = ydata - yfit
419         chi2 = np.sum(resid**2/self.RMS_obs[i]**2)
420         # RMS_res = np.sqrt(np.sum(resid**2))
421
422         # saving the fit parameters
423         self.fit_A[i] = popt[0]
424         self.fit_x0[i] = popt[1]
```

```
425             self.fit_chi2[i] = chi2
426             self.mock_fit_spec[i] = fit_mock_spec
427 
428             return
429 
430 
431 
432         ### extension functions ###
433 
434         # mock fitting 'function'
435         def mock_fun(self, X, A, x0):
436 
437             # identification of model to use
438             i = self.ind
439 
440             # mock spectrum
441             mock_spec = self.mock_spec[i]
442 
443             # mock values
444             xmock = mock_spec['vel'].values
445             ymock = mock_spec['flux'].values
446 
447             # mock values
448             xmock = xmock + x0
449             ymock = ymock
450 
451             # interpolated 'function'
452             Y = np.interp(X, xmock, ymock)
453 
454             return A * Y
455 
456 
457 
458         ## generating surface brightness profile
459         def gen_sb_prof(self, ind = None):
460 
461             # identification of model to use
462             i = self.ind
463             if ind:
464                 i = ind
465 
466             # returning surface brightness profile
467             return Sersic1D.evaluate(self.rad_prof, 1, self.r_SB[i], n = 1)
468 
469 
470 
471         def save_model_params(self, save_file = True):
472 
473             self.params['A'] = self.fit_A
474             self.params['x0'] = self.fit_x0
475             self.params['chi2'] = self.fit_chi2
476 
477             if save_file:
478                 # saving table with parameters of models
479                 self.params.to_csv(f'{self.mocks_dir}/G{self.id[0]}
```

```
                                        _model_params.txt', index = False)
480
481         return
482
483
484
485     def best_fit(self):
486
487         # retrieving index of best fit mock
488         idx = self.params.index[self.params['chi2'] == self.params['
                                    chi2'].min()].tolist()[0]
489
490         # getting name of the best fit mock files
491         filename_best = self.params['filename'][idx]
492
493         # directory for best fit mock files
494         best_fit_dir = './Data/Processed/Mocks/CO/Best_fit'
495
496         # copying best fit files to best fit directory
497         sh.copyfile(f"{self.mocks_dir}/{filename_best}_obs_comp.png", f
                                    "{best_fit_dir}/G{self.id[0]}
                                    _model_obs_comp.png")
498         sh.copyfile(f"{self.mocks_dir}/{filename_best}_profiles.png", f
                                    "{best_fit_dir}/G{self.id[0]}
                                    _model_profiles.png")
499         sh.copyfile(f"{self.mocks_dir}/{filename_best}.txt", f"{
                                    best_fit_dir}/G{self.id[0]}_model.txt")
500
501         # returning specified values of best fit
502         inc_best = self.params['inc'][idx]
503         A_best = self.params['A'][idx]
504         x0_best = self.params['x0'][idx]
505
506         return idx, inc_best, A_best, x0_best
```